Remote detection of cyanobacteria blooms in an optically shallow subtropical lagoonal estuary using MODIS data

Jennifer P. Cannizzaro[a*], Brian B. Barnes[a], Chuanmin Hu[a], Alina A. Corcoran[b], Katherine A. Hubbard[b], Eric Muhlbach[b], William C. Sharp[c], Larry E. Brand[d], Christopher R. Kelble[e]

[a]*College of Marine Science, University of South Florida, St. Petersburg, FL 33701, U.S.A.*

[b]*Fish and Wildlife Research Institute, Florida Fish and Wildlife Conservation Commission, St. Petersburg, FL 33701, U.S.A.*

[c]*Fish and Wildlife Research Institute, Florida Fish and Wildlife Conservation Commission, Marathon, FL 33050, U.S.A.*

[d]*Rosenstiel School of Marine and Atmospheric Science, University of Miami, Miami, FL 33149, U.S.A.*

[e]*U.S. NOAA Atlantic Oceanographic & Meteorological Laboratory, Miami, FL 33149, U.S.A.*

[*]Corresponding author – e-mail: jpatch@mail.usf.edu, tele: (727)-553-3954

ABSTRACT

Widespread and persistent Ecosystem Disruptive Algal Blooms dominated by marine picocyanobacteria (*Synechococcus*) commonly occur in the subtropical lagoonal estuary of Florida Bay (U.S.A). These blooms have been linked to a decline in natural sheet flow over the past century from upstream Everglades National Park. Remote sensing algorithms for monitoring cyanobacteria blooms are highly desired but have been mainly developed for freshwater and coastal systems with minimal bottom reflectance contributions in the past. Examination of in situ optical properties revealed that *Synechococcus* blooms in Florida Bay exhibit unique spectral absorption and reflectance features that form the basis for algorithm development. Using a large, multi-year match-up dataset (2002-2012; n=682) consisting of in situ pigment concentrations and Moderate Resolution Imaging Spectroradiometer (MODIS) Rayleigh-corrected reflectance ($R_{rc}(\lambda)$), classification criteria for detecting cyanobacteria blooms with chlorophyll-a concentrations (Chl-a) ~5-40 mg m^{-3} were determined based on a new approach to combine the MODIS Cyanobacteria Index, CI_{MODIS}, and spectral shape around 488nm, SS(488). The inclusion of SS(488) was required to prevent false positive classifications in seagrass-rich, non-bloom waters with high bottom reflectance contributions. 75% of cyanobacteria blooms were classified accurately based on this modified CI approach with <1% false positives. A strong correlation observed between cyanobacteria bloom in situ Chl-a and CI_{MODIS} (r^2=0.80, n=32) then allowed cyanobacterial chlorophyll-a concentrations (Chl_{CI}) to be estimated. Model simulations and image-based analyses showed that this technique was insensitive to variable aerosol properties and sensor viewing geometry. Application of the approach to the entire MODIS time-series (2000 - present) may help identify factors controlling blooms and system responses to ongoing management efforts aimed at restoring flow to pre-drainage conditions.

The method may also provide insights for algorithm development for other lagoonal estuaries that experience similar blooms.

Keywords: Algal bloom; Ocean color; Remote sensing; MODIS; Chlorophyll; Cyanobacteria; *Synechococcus*; Florida Bay

1. Introduction

Florida Bay (Florida, USA) is a shallow (<3m), subtropical lagoonal estuary located at the southern tip of Everglades National Park (ENP). Once known for its pristine, oligotrophic waters, this region experienced a cascade of ecological disturbances beginning in the late 1980's, including seagrass die-offs, increased turbidity, and frequent and prolonged picocyanobacteria blooms followed by declines in sponge and spiny lobster populations (Butler et al. 1995; Fourqurean and Robblee 1999; Hall et al. 1999; Hall et al. 2016; Wall et al. 2012). Much of this ecological damage has been linked to extensive canal construction in ENP beginning in the 1920's to alleviate flooding for South Florida agricultural lands (Light and Dineen 1994). The resultant reduction in natural freshwater flow via Taylor Slough led to longer residence times and occasional periods of intense hypersalinity (Fourqurean and Robblee 1999; Kelble et al. 2007; Nuttle et al. 2000; Rudnick et al. 2005). Efforts to restore natural sheet flow are currently underway as part of the federally mandated Comprehensive Everglades Restoration Plan (CERP; https://www.nps.gov/ever/learn/nature/cerp.htm).

Picocyanobacteria blooms in Florida Bay are dominated by *Synechococcus*, a small (~2µm), unicellular marine genus found ubiquitously throughout much of the world's oceans (Waterbury et al. 1979). Genetic analysis revealed high similarities with coastal strains belonging

64 to Clade VIII that contain the light-harvesting pigment phycocyanin (PC) (Berry et al. 2015).
65 These blooms often persist from months to years, extend up to hundreds of square kilometres,
66 and exhibit chlorophyll-a concentrations (Chl-a) up to ~40 mg m^{-3} (Glibert et al. 2009; Phlips
67 and Badylak 1996; Phlips et al. 1999). Extreme bloom populations comprise >99% of total
68 phytoplankton biovolume and exhibit cell abundances $>10^6$ cells ml^{-1} (Phlips and Badylak 1996;
69 Phlips et al. 1999). Increased light attenuation, anoxic events, and reduced zooplankton grazing
70 are commonly associated with these Ecosystem Disruptive Algal Blooms (Goleski et al. 2010;
71 Phlips and Badylak 1996; Phlips et al. 1999).
72 Florida Bay picocyanobacteria blooms were first reported throughout much of the 1990's
73 (Boyer et al. 1999; Phlips et al. 1999) and have since occurred in 2002, 2003, and 2005-2008
74 (Berry et al. 2015; Brand et al. 2010; Evans et al. 2006; Gardner and McCarthy 2009; Glibert et
75 al. 2004; Glibert et al. 2009; Goleski et al. 2010). The 2005-2008 bloom was particularly
76 noteworthy given its wide expanse and extended duration. Also, bloom populations were
77 observed for the first time in the historically clear waters of northeastern Florida Bay. More
78 recently, major bloom events were reported in 2013 and 2016 (unpublished data, Florida Fish
79 and Wildlife Conservation Commission's Fish and Wildlife Research Institute (FWC-FWRI)).
80 Several hypotheses have been proposed regarding potential nutrient sources that may serve as
81 drivers for these blooms (Hitchcock et al. 2007). Linkages between bloom occurrence and
82 tropical storm frequency and global climatic indices have also been made (Briceño and Boyer
83 2009). However, despite increased water quality monitoring efforts over the past several decades
84 (Boyer et al. 1999; Boyer et al. 2009), nutrients sources responsible for maintaining these blooms
85 remain a topic of debate.

Field-based phytoplankton monitoring programs offer a high degree of specificity by providing information on phytoplankton type (often to the genus or species level) and abundance, but they are often costly, labour intensive, and fail to adequately report on fine-scale spatial and temporal distribution patterns (Rantajärvi et al. 1998). Satellite remote sensing with larger spatial coverage and higher temporal resolution can complement traditional water sampling efforts by providing timely information on phytoplankton bloom dynamics. Global oceanic bio-optical algorithms for retrieving Chl-a (used as a proxy for phytoplankton biomass) often fail in optically complex coastal, estuarine, and inland environments and are incapable of differentiating between different bloom types (Carder et al. 1991; Wozniak and Stramski 2004). Hence, the development of alternative approaches for detecting specific bloom types has been actively pursued over the past several decades (Blondeau-Patissier et al. 2014; Cullen et al. 1997). Of these, several algorithms for detecting PC-containing cyanobacteria blooms have been developed, but mainly for freshwater bloom-forming genera (*Microcystis*, *Planktothrix*, *Anabaena*, *Aphanizomenon*) (Dekker 1993; Hunter et al. 2009; Qi et al. 2014; Schalles and Yacobi 2000; Simis et al. 2005; Wynne et al. 2013; Wynne et al. 2008).

The development of remote sensing algorithms requires knowledge of the inherent optical properties (IOPs; or spectral absorption, $a(\lambda)$, and backscattering, $b_b(\lambda)$, coefficients) of water column constituents that influence the color of the water as quantified by remote sensing reflectance, $R_{rs}(\lambda)$. These optically active constituents mainly include phytoplankton, detrital material, minerals, colored dissolved organic matter (CDOM), and pure water. Because phytoplankton, detritus, and CDOM absorb blue light strongly and pure water and phytoplankton absorb red light strongly, elevated reflectance often occurs at green wavelengths in coastal, estuarine, and inland environments (Kirk 1994). Inorganic suspended sediments, especially those

109 with high mineral content, strongly scatter light, causing reflectance to increase at all
110 wavelengths. In shallow areas with relatively low light attenuation, radiance reflected by the
111 bottom can also impact $R_{rs}(\lambda)$ (Lee et al. 2001).

112 Florida Bay presents a particularly challenging case for remote sensing of cyanobacteria
113 blooms given its optical complexity compounded by its shallow nature and close proximity to
114 land. Compared to nearby river-dominated estuaries, Florida Bay is less heavily influenced by
115 direct terrestrial freshwater runoff, leading to lower CDOM loading (Maie et al. 2006). Light
116 attenuation is relatively low and mainly dominated by tripton (non-algal particulate material),
117 except for during blooms when phytoplankton can be important (Kelble et al. 2005; Phlips et al.
118 1995). Increased light penetration in weakly attenuating waters often leads to high bottom
119 reflectance contributions that can negatively impact accuracies of bio-optical algorithms (Blakey
120 et al. 2016; D'Sa et al. 2002). Chl-a algorithm retrieval accuracies for this region are further
121 susceptible to increased turbidity (Cannizzaro et al. 2013b) that may occur over short durations
122 (days to weeks) following storm events (Conmy et al. 2009) or longer durations (months to
123 years) following seagrass die-off events (Barnes et al. 2014; Stumpf et al. 1999). Algorithm
124 failure caused by atmospheric correction errors attributed to absorbing aerosols and straylight
125 contamination may also occur (Feng and Hu 2017; Mouw et al. 2015). Optical differentiation
126 between various phytoplankton bloom types is another challenge for Florida Bay where seasonal
127 diatom blooms also occur (Jurado et al. 2007; Phlips and Badylak 1996; Phlips et al. 1999;
128 Richardson 2009).

129 Given the lack of reliable remote sensing algorithms for quantifying cyanobacteria
130 blooms in Florida Bay, the objectives of this study were to (1) characterize the bio-optical
131 properties of this system, (2) develop and evaluate a remote sensing approach for classifying and

quantifying cyanobacteria blooms, and (3) apply this new method to examine the 2005-2008 bloom event. The fundamental reasons behind why the new approach works are examined, and both strengths and weaknesses of the approach are presented. Finally, recommendations for future work using alternative sensors aimed at improving bloom detection in Florida Bay and other lagoonal estuaries where these blooms are known to occur are provided.

2. Background on algorithm development

Remote sensing algorithms for detecting freshwater cyanobacteria blooms commonly target the dip in $R_{rs}(\lambda)$ at ~625nm caused by PC absorption (Dekker 1993; Hunter et al. 2009; Qi et al. 2014; Schalles and Yacobi 2000; Simis et al. 2005; Wynne et al. 2013; Wynne et al. 2008). The European Space Agency's Medium Resolution Imaging Spectrometer (MERIS) aboard the ENVISAT mission (2002-2012) and Ocean and Land Colour Instrument (OLCI) aboard the Sentinel 3A (2016-) and Sentinel 3B (2018-) missions included a 620nm waveband, permitting detection of this feature at 300m spatial resolution. However, the four year gap between the end of the MERIS mission and start of the Sentinel 3A mission interrupts the creation of a long-term (multi-decadal) ocean color data record. The U.S. NASA Moderate Resolution Imaging Spectroradiometers (MODIS) aboard the Terra (2000-) and Aqua (2002-) missions provide a more continuous stream of ocean color data twice daily at 250-1000m spatial resolution, but waveband placement for these sensors is inadequate for measuring the PC reflectance dip at 625nm (Kutser et al. 2006).

Alternative bloom detection algorithms use a baseline subtraction approach to target the weak chlorophyll fluorescence efficiency and enhanced scattering exhibited by cyanobacteria blooms at red and near-IR wavebands (Moore et al. 2017). For example, the MERIS

155 Cyanobacteria Index (CI_{MERIS}) utilizes a three-band spectral shape algorithm, SS(λ), to quantify
156 the height of $R_{rs}(\lambda)$ at 681nm relative to a baseline formed linearly between two adjacent
157 wavebands (665nm and 709nm) (Wynne et al. 2010; Wynne et al. 2008). Baseline subtraction
158 algorithms have also been used for several other ocean color applications (Gower et al. 2004; Hu
159 2009; Letelier and Abbott 1996; Matthews et al. 2012; Qi et al. 2014). This is because they are
160 less impacted by atmospheric correction errors and changes in aerosols and observing conditions
161 compared to band-ratio methods (Hu 2009). Such errors are linearly proportional to wavelength
162 to first order and can therefore be subtracted.
163 Another example is the MERIS Maximum Peak Height (MPH) algorithm that quantifies
164 phytoplankton biomass based on the height above a spectral baseline formed linearly between
165 Rayleigh-corrected reflectance, $R_{rc}(\lambda)$, at 664nm and 885nm where maximal $R_{rc}(\lambda)$ at 681, 709,
166 or 753nm occurs (Matthews et al. 2012; Matthews and Odermatt 2015). High biomass
167 (Chl_MPH > 20 mg m^{-3}) cyanobacteria-dominated blooms are then distinguished from
168 eukaryotic blooms using additional spectral shapes that target sun-induced chlorophyll
169 fluorescence (SICF; 664-681-709nm), sun-induced phycobilipigment (PC and allophycocyanin)
170 fluorescence (SIPF; 620-664-681nm), and backscatter and absorption induced reflectance
171 (BAIR; 665-709-885nm). The benefit of using $R_{rc}(\lambda)$, which includes a partial atmospheric
172 correction to correct for gaseous absorption and Rayleigh (molecular) scattering effects, instead
173 of the commonly used $R_{rs}(\lambda)$ is because 1) atmospheric correction schemes can add uncertainties
174 over coastal, estuarine, and inland regions due to incorrect assumptions (e.g., negligible water
175 signal in the near-infrared, relationship between different spectral bands used in the iterative
176 atmospheric correction) and 2) the standard atmospheric correction scheme used by NASA
177 SeaDAS data processing software often generates a data mask over shallow and/or turbid waters.

178 Although adaptation of the MERIS MPH algorithm for use with MODIS data is not
179 possible because of the requirements on extra bands at 620- and 709-nm, CI_{MERIS} was adapted
180 for use with MODIS $R_{rc}(\lambda)$ using the same baseline subtraction approach, providing continuity
181 among sensors following the end of the MERIS mission (Wynne et al. 2013). Wavebands for
182 deriving the MODIS Cyanobacteria Index, CI_{MODIS}, are the same as those used for determining
183 MODIS Fluorescence Line Height (FLH) (667, 678, and 748nm); and CI_{MODIS} is essentially the
184 negative of MODIS FLH. MODIS FLH is commonly used as an indicator of coastal and
185 estuarine eukaryotic algal blooms (Gower et al. 2004; Hu et al. 2005). Despite oversaturation of
186 CI_{MODIS} for extreme cyanobacteria blooms in freshwater systems where highly vacuolated cells
187 aggregate at the surface forming vast dense mats, CI_{MODIS} provided comparable results to
188 CI_{MERIS} (Wynne et al. 2013).
189 CI_{MODIS} has been successfully applied not only to freshwater *Microcystis* blooms (Zhang
190 et al. 2017), but also to blooms dominated by filamentous cyanobacteria (*Nodularia*) in brackish
191 waters of the Caspian Sea (Moradi 2014). However, the performance of the CI_{MODIS} algorithm
192 for blooms dominated by marine genera (*Synechococcus*) in optically complex, coastal lagoons
193 prone to high bottom reflectance contributions (Florida Bay) has been found to yield too many
194 false positives, making it necessary to modify this approach.
195
196 3**. Data and Methods**
197 ***3.1 Study area***
198 Florida Bay (2,200 km^2) is a triangular-shaped lagoonal estuary bounded to the north by
199 mainland Florida, to the south by the Florida Keys, and to the west by the western boundary of
200 ENP (Fig. 1). Coastal waters west of Florida Bay are considered part of Greater Florida Bay

(GFB). East of Florida Bay are several shallow (<3m), oligotrophic lagoons (Blackwater Sound, Manatee Bay, and Barnes Sound; or BMB). The geomorphology of Florida Bay consists of a complex series of sub-basins separated by shallow subtidal to intertidal carbonate mud banks (<1 m). Wind forcing is the primary driver of water renewal for all regions within Florida Bay and flow among basins occurs through narrow tidal channels and across the shallow mud banks (Lee et al. 2006; Lee et al. 2008; Lee et al. 2016). Seagrass communities cover much of Florida Bay with increasing densities observed from the northeast to southwest (Zieman et al. 1989), and while coverage is generally stable, periodic localized and sometimes widespread mortality events have occurred (Hall et al. 2016).

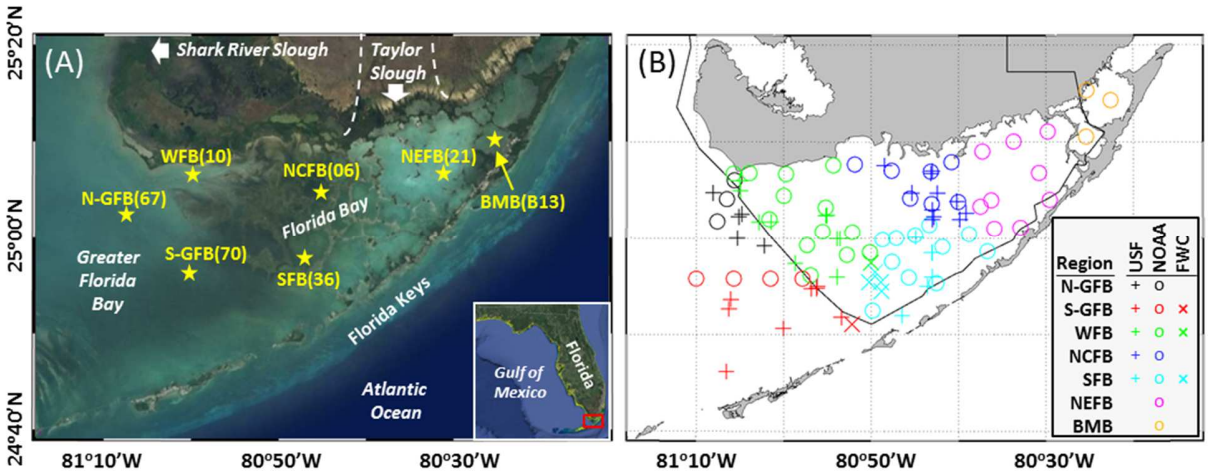

Figure 1. (A) Landsat image of Florida Bay and adjacent water bodies collected on 30 December 2016. Most regions in Florida Bay are less than 2m deep with many areas less than 1m. Star symbols show locations of MODIS time-series stations. Abbreviations: N-GFB= Northern Greater Florida Bay; S-GFB = Southern Greater Florida Bay; WFB = West Florida Bay, NCFB=North Central Florida Bay, SFB = South Florida Bay, NEFB = Northeast Florida Bay, and BMB = Blackwater Sound, Manatee Bay, and Barnes Sound. NOAA station numbers are included in parenthesis. (B) Map of study area showing in situ station locations sorted by region for three independent field data sets: + = USF (1997-1998), ○ = NOAA (2002-2012, 2016), and X = FWC (late-2013). The solid black line represents the southern boundary for Everglades National Park.

Florida Bay and adjacent water bodies can be divided into seven distinct subregions (Fig. 1) with variable nutrient loading, circulation, tidal characteristics, and bottom substrates that lead

to variable optical properties and the dominance of different phytoplankton groups (Boyer et al. 1997; Boyer et al. 2009; Glibert et al. 2009; Hitchcock et al. 2007; Lee et al. 2006; Lee et al. 2008; Phlips et al. 1995; Phlips and Badylak 1996; Rudnick et al. 1999; Smith 1997).

West Florida Bay (WFB) and GFB are strongly influenced by mixing between bay waters and marine inflows from the Gulf of Mexico. In Northern Greater Florida Bay (N-GFB) and northern WFB, seagrass density is sparse or absent and waters are often turbid (Kelble et al. 2005; McPherson et al. 2011). Decadal trends in $R_{rs}(\lambda)$ obtained from the Advanced Very High Resolution Radiometer (AVHRR) (Stumpf et al. 1999) and Landsat-5 Thematic Mapper (TM) (Barnes et al. 2014) showed increased reflectance indicative of high sediment resuspension following major seagrass die-off events. Here, diatoms often dominate phytoplankton community composition with blooms commonly occurring from late-summer to winter (Jurado et al. 2007; Phlips and Badylak 1996; Phlips et al. 1999; Richardson 2009).

Southern Greater Florida Bay (S-GFB) and southern portions of WFB include vast areas of dense seagrass beds. Light attenuation is relatively low in these regions because seagrass beds help to stabilize sediments by dampening tidal and wind energy (Kelble et al. 2005; McPherson et al. 2011). MODIS $R_{rs}(\lambda)$ is often low as a result of increased light penetration and low bottom albedos that are characteristic of seagrass beds (Gao et al. 2007; Lee et al. 2001).

North Central Florida Bay (NCFB) is the most geomorphologically isolated region with influxes of marine and freshwater restricted by the configuration of mud banks. Residence times here are on the order of 6-12 months (Lee et al. 2006; Lee et al. 2008). While median Chl-a in NCFB and WFB are both relatively high (~1.2-1.3 mg m^{-3}, respectively) (Boyer et al. 2009), bloom-forming phytoplankton communities differ greatly with picocyanobacteria (*Synechococcus*) often dominating in NCFB compared to diatoms in northern WFB (Glibert et

247 al. 2009; Hitchcock et al. 2007; Phlips and Badylak 1996; Phlips et al. 1999). Nitrogen limitation
248 to the west and phosphorus limitation to the east gives way to a central convergence zone in this
249 region favouring the growth of picocyanobacteria (Brand 2002; Brand et al. 2010). During
250 summer, these blooms often originate in NCFB and then spread to South Florida Bay (SFB) in
251 fall and early-winter when passing cold fronts cause a shift in wind direction to the north, forcing
252 waters to the south (Lee et al. 2016; Phlips et al. 1999). In the absence of blooms, low light
253 attenuation and median Chl-a (0.5 mg m^{-3}) are generally observed in SFB (Boyer et al. 2009;
254 Kelble et al. 2005).
255 Northeast Florida Bay (NEFB) is characterized by relatively large basins separated by
256 narrow banks. This region is more isolated from tidal and oceanic exchange processes compared
257 to the rest of Florida Bay (Smith 1997). Phosphorus limitation is the main factor limiting
258 phytoplankton growth in this region as reflected by relatively low median Chl-a (0.4 mg m^{-3})
259 (Boyer et al. 2009). Seasonal freshwater influxes from Taylor Slough lead to nitrogen-rich
260 waters that favour the growth of mixtures of diatoms, cyanobacteria, microflagellates, and
261 dinoflagellates (Hitchcock et al. 2007). Sparse seagrass coverage makes this area susceptible to
262 frequent sediment resuspension events from wind and wave action. This results in high
263 reflectance year round (Stumpf et al. 1999), leading to saturation problems for MODIS $R_{rs}(\lambda)$
264 when using standard atmospheric correction algorithms (Gao et al. 2007).
265 Mean Chl-a in BMB from 1995-2004 was also relatively low (0.4 mg m^{-3}) and
266 phytoplankton populations prior to the 1990's were dominated by diatoms and dinoflagellates
267 (Phlips et al. 1999). In 2005-2008, a widespread picocyanobacteria bloom persisted for several
268 years attributed to hurricane activity and a local road widening project (Glibert et al. 2009). This

major bloom event led to a regime shift with higher mean Chl-a (0.8 mg m^{-3}) observed the five years following the bloom (Millette et al. 2018).

3.2 Field measurements

Three independent field data sets were used in this study (Fig. 1b):

(1) Chl-a, spectral absorption, and $R_{rs}(\lambda)$ measurements obtained by the University of South Florida (USF) in 1997-1998 were used to characterize the optical properties of Florida Bay and Greater Florida Bay. Field excursions lasting 1-3 days were conducted in January, May, October, and November 1997 and January 1998 (Table 1). Water column depths ranged from 0.8m to 3.4m. Bottom types varied from dense seagrass to mud or sand and were often visible to the naked eye.

Table 1. Summary of Florida Bay field measurements collected in 1997-1998.

Date(s)	Regions	Stations	Chl-a	$a_p(\lambda)$	$a_d(\lambda)$	$a_{CDOM}(\lambda)$	$R_{rs}(\lambda)$
19,22 Jan 1997	S-GFB, WFB, NCFB, SFB	10	✓	✓	✓	-	✓
1-2 May 1997	S-GFB, NCFB	4	✓	✓	✓	-	✓
2-4 Oct 1997	N-GFB, S-GFB, WFB, NCFB, SFB	18	✓	✓	✓	✓	✓
4 Nov 1997	S-GFB, WFB	4	✓	✓	✓	✓	✓
29-31 Jan 1998	N-GFB, WFB, NCFB, SFB	12	✓	✓	✓	✓	✓

Surface grab samples were stored on ice until returned to shore and processed the same day. Absorption spectra of total particulate, $a_p(\lambda)$, and detrital, $a_d(\lambda)$, material was measured using the quantitative filter technique (Kiefer and SooHoo 1982; Yentsch 1962) with a custom-built, 512-channel spectroradiometer (Spectrix; ~330-880 nm). Pigments were extracted using hot methanol (Kishino et al. 1985) and Chl-a was determined fluorometrically on these pigment

288 extracts with a Turner-Designs 10-AU Field Fluorometer (Holm-Hansen and Riemann 1978).
289 Phytoplankton absorption spectra, $a_{ph}(\lambda)$, was calculated by subtracting $a_d(\lambda)$ from $a_p(\lambda)$.
290 Chlorophyll-specific phytoplankton absorption, $a^*_{ph}(\lambda)$, was determined by normalizing $a_{ph}(\lambda)$ to
291 Chl-a. Absorption spectra of CDOM, $a_{CDOM}(\lambda)$, was determined from 0.2µm seawater filtrates
292 with a Perkin-Elmer Lambda 18 spectrophotometer using a 10cm pathlength cell and purified
293 water as a reference. Total absorption spectra, $a_t(\lambda)$, was calculated as the sum of individually
294 measured absorption components ($a_{ph}(\lambda)$, $a_d(\lambda)$, $a_{CDOM}(\lambda)$) and pure water absorption, $a_w(\lambda)$ (Pope
295 and Fry 1997).
296 $R_{rs}(\lambda)$ was determined from above-water hyperspectral measurements of upwelled total
297 radiance, downwelled sky radiance, and the radiance reflected from a standard diffuse reflector
298 (Spectralon; 10%). These measurements were obtained using a custom spectroradiometer
299 (Spectrix). Data collection and processing methods are described further in Lee et al. (2010).
300 (2) A large, multi-year pigment dataset (2002-2012; n=3,362) collected as part of NOAA
301 Atlantic Oceanographic Meteorological Laboratory's (NOAA-AOML) South Florida Program
302 was used for algorithm development. Surface seawater samples were collected for Chl-a from
303 fifty stations located in GFB (n=7), Florida Bay (n=40), and BMB (n=3) at frequencies ranging
304 from biweekly to quarterly with increased sampling during major bloom events. PC
305 concentrations were measured in Florida Bay during the majority of these field excursions with
306 samples processed by the University of Miami. All pigment samples were filtered onto Whatman
307 GF/F filters and stored at -20^{o}C until processed. Chlorophyll-a was extracted overnight using a
308 60:40 90% acetone to dimethyl sulfoxide mixture and determined fluorometrically (Shoaf and
309 Lium 1976). PC was extracted overnight at 5 ^{o}C with a phosphate buffer (0.05 M H_2KPO_4, 0.05
310 M HK_2PO_4; pH 6.5; with 0.01% (v/v) mercaptoethanol added) and concentrations were

311 determined with a SPEX Fluorolog-3 spectrofluorometer using 580nm excitation and 640nm
312 emission.
313 Chl-a was also measured in Florida Bay by NOAA-AOML on 28-29 September 2016,
314 but PC concentrations were not determined. Instead, PC fluorescence (in relative fluorescence
315 units, RFU) was measured with a YSI EXO Total Algae PC Smart Sensor. This data was used to
316 evaluate the performance of the new algorithm.
317 (3) Pico- and nanocyanobacteria cell concentrations quantified using flow cytometry as
318 part of event response and monitoring efforts by FWC-FWRI were used for algorithm validation.
319 Weekly to biweekly seawater samples were collected in Florida Bay between October 3 and
320 November 21, 2013. Surface grab samples were pre-filtered through 64 µm mesh and 1.5 ml
321 aliquots were immediately preserved with glutaraldehyde (0.1% final concentration). Samples
322 were flash frozen with liquid nitrogen, stored at -80° C and processed within five months of
323 collection with an Accuri C6 flow cytometer (BD Biosciences, San Jose, CA) equipped with a
324 16µm aperture and standard detectors and filters. Standard flow cytometric methods were used
325 for determination of cyanobacteria abundance (Marie et al. 1997; Marie et al. 2005). Seawater
326 samples were diluted with sterile filtered seawater as needed to ensure that sampling rates were
327 below the instrument's maximum event capacity (10,000 events $second^{-1}$). Sterile seawater
328 blanks and a replicate 1.5 ml aliquot for a subset of eight samples were also evaluated. The
329 abundance of pico- and nano-cyanobacteria was determined using FCS Express 4 flow cytometry
330 software (DeNovo Software, Glendale, CA) based on size (0.79-2 µm for picoplankton, 2-16 µm
331 for nanoplankton) and red and orange autofluorescence characteristics. Beads of standard sizes
332 (0.79 -16 µm) and size and fluorescence properties obtained from a Gulf of Mexico

Synechococcus sp. (CCMP836) isolate as well as prior studies (e.g., Gérikas Ribeiro et al. 2016; Phlips et al. 1999) informed gating of flow cytometric biplots from field samples.

3.3 Satellite data

Level-0 MODIS Terra and Aqua data were downloaded from the U.S. NASA Goddard Space Flight Center (GSFC) and processed using SeaDAS (version 7.4, with calibration settings matching GSFC reprocessing 2018.0) to generate $R_{rc}(\lambda)$ (dimensionless) at 11 wavebands as well as Level-2 Processing Flags (l2_flags). The ocean bands centered at 412, 443, 488, 531, 547, 667, 678, and 748 nm have 10nm bandwidths and 1 km nadir resolutions. The land bands centered at 469 (459–479) and 555 (545–565) nm have 500 m resolution, and the land band centered at 645 (620–670) nm has 250 m resolution. MODIS data were mapped to a cylindrical equidistant projection at 250m resolution for further analysis. $R_{rc}(\lambda)$ data at 645nm, 555nm, and 469nm were used to generate "true color" Red-Green-Blue (RGB) composite imagery for visual inspection. Mud banks were masked in classified imagery based on the 1997 Florida Bay bottom types map (Prager and Halley 1997).

3.4 Bloom definitions

A constant and conservative threshold of Chl-a was used to distinguish between bloom (>5 mg m^{-3}) and non-bloom (<5 mg m^{-3}) conditions despite it being well established that Chl-a bloom thresholds in Florida Bay change significantly over both space and time (Millette et al. 2018; Nelson et al. 2017). Cyanobacteria blooms were further separated from 'other' (non-PC containing) blooms in a variety of ways depending on the in situ dataset. Although it would have been ideal to utilize a single definition for what constitutes a cyanobacteria bloom in this study,

356 the different measurements collected by the different institutions/agencies required some
357 flexibility on this issue. For the 1997-1998 field data (USF), information on phytoplankton
358 taxonomy was not available, so microscopy measurements obtained near-concurrently as part of
359 an independent field study were used to identify the nature of bloom populations (Phlips et al.
360 1999). For the 2002-2012 and 2016 field data (NOAA-AOML), cyanobacteria blooms were
361 identified based on PC > 0 mg m^{-3} and PC fluorescence > 0.5 RFU, respectively. The slight
362 increase for the PC fluorescence threshold was because of known interference of PC
363 fluorescence probe readings caused by turbidity (Zamyadi 2011). For the 2013 field data (FWC-
364 FWRI), cyanobacteria blooms were defined based on total pico- and nano-cyanobacteria cellular
365 abundances that were binned as follows: 'high' bloom (>10^7 cells ml^{-1}), 'medium' bloom (10^6-
366 10^7 cells ml^{-1}), 'low' bloom ($0.45x10^6$-10^6 cells ml^{-1}), and non-bloom (<$0.45x10^6$ cells l^{-1}).
367
368 ***3.5 Match-up comparisons***
369 The following criteria were used to find co-located and near-concurrent in situ Chl-a and
370 MODIS $R_{rc}(\lambda)$ data for algorithm development and validation. Both measurements had to be
371 collected on the same day. Reducing the temporal window to the standard +/- 3 hours was
372 considered unnecessary given the long residence times for this system and would have reduced
373 the number of match-up pairs, compromising the robustness of the dataset. Center pixels were
374 extracted only instead of a 3x3 or 5x5 means about the center because of close proximity to land
375 and mud banks for many of the stations. Pixels flagged for land, clouds, and high radiance were
376 discarded. A cloud mask was applied following the approach of Hu (2011) by using thresholds of
377 several MODIS bands.

For algorithm development using the 2002-2012 field data, valid MODIS $R_{rc}(\lambda)$ were found for ~20% (n=682) of available in situ Chl-a. Match-up success was greatest in N-GFB, S-GFB, WFB, and SFB (25-29%) compared to NCFB (17%) and NEFB and BMB (6-7%). High radiances and proximity to land rendered much of the latter satellite data invalid. A higher percentage of match-up pairs was also found in fall and winter (26-28%) compared to spring and summer (15-16%).

Out of the 682 valid match-up pairs, a total of 41 bloom (Chl-a > 5 mg m^{-3}) and 641 non-bloom (Chl-a < 5 mg m^{-3}) match-up pairs were found. These blooms spanned across seven different years (2002, 2003, 2005-2008, and 2010) and sixteen individual MODIS scenes. The majority of blooms were dominated by cyanobacteria (Chl-a > 5 mg m^{-3}, PC > 0 mg m^{-3}; n=32) and mainly occurred in NCFB and SFB. Match-up pairs for nine 'other' blooms (Chl-a > 5 mg m^{-3}, PC = 0 mg m^{-3}) were also identified with stations located in N-GFB and northern WFB. Although these latter blooms were likely dominated by diatoms based on previous studies (Jurado et al. 2007; Phlips and Badylak 1996; Phlips et al. 1999; Richardson 2009), taxonomic measurements to support this hypothesis were unavailable.

3.6 Spectral shape algorithm

Spectral shapes were determined by

$$SS(\lambda) = \left[R(\lambda) - R(\lambda^-) - \{R(\lambda^+) - R(\lambda^-)\} \times \frac{(\lambda-\lambda^-)}{(\lambda^+-\lambda^-)}\right] \quad (1)$$

where R was either in situ $R_{rs}(\lambda)$ (sr^{-1}) or MODIS $R_{rc}(\lambda)$ (dimensionless). In situ $R_{rs}(\lambda)$ were convolved to MODIS spectral bandwidths using the instrument- and band-specific relative spectral response functions prior to calculating spectral shapes. For CI_{MODIS}, λ^- = 667nm, λ=678nm, and λ^+ = 748nm; and CI_{MODIS} = -SS(678) (Wynne et al. 2013).

3.7 Accuracy assessment

Algorithm accuracy was assessed using a confusion matrix (Kohavi and Provost 1998), whereby in situ reference data identified as either a cyanobacteria bloom (cb) or non-cyanobacteria bloom (ncb) (including 'other' blooms and non-blooms) was classified as a cyanobacteria bloom (CB) or non-cyanobacteria bloom (NCB). Based on this system, each match-up pair was identified as either a (A) true positive (cb-CB), (B) false negative (cb-NCB), (C) false positive (ncb-CB), or (D) true negative (ncb-NCB).

Precision was determined as the percentage of true blooms among the area identified as blooms (A/(A+C)). Sensitivity was the percentage of true blooms that were correctly identified (A/(A+B)). Overall algorithm performance was determined based on the F-measure coefficient (FM), which is essentially the harmonic mean between precision and sensitivity, and is calculated as follows:

$$FM = \frac{(\beta^2+1)\times precision \times sensitivity}{\beta^2 \times precision + sensitivity} \quad (2)$$

For β=1, equal weight is given to precision and sensitivity. In this study, β was set to 0.5 to give precision more weight than sensitivity.

4. Results

4.1 Bio-optical properties of Florida Bay

In situ Chl-a and spectral absorption properties were highly variable in Florida Bay between 1997 and 1998, with Chl-a ranging from 0.3 to 17 mg m^{-3}, $a_{ph}(443)$ ranging from 0.02-0.88 m^{-1}, $a_d(443)$ ranging from 0.01-0.62 m^{-1}, and $a_{CDOM}(443)$ ranging from 0.14-0.75 m^{-1} (Table 2, Fig. 2). Mean Chl-a was higher in N-GFB, WFB, and NCFB (>4 mg m^{-3}) compared to S-GFB

and SFB (<4 mg m^{-3}) consistent with previous reports (Boyer et al. 1997; Boyer et al. 2009; McPherson et al. 2011; Nelson et al. 2017; Phlips et al. 1995). Weak to moderate phytoplankton blooms with Chl-a ranging from ~5-17 mg m^{-3} were observed in WFB in January 1997 (n=4) and NCFB and SFB in October 1997 (n=5). Because phytoplankton taxonomy was not determined during these field surveys, microscopy results obtained near-concurrently as part of an independent field study were used to identify the nature of these bloom populations as being dominated by diatoms and cyanobacteria (*Synechococcus*), respectively (Phlips et al. 1999). Each of these blooms persisted for several months, providing confidence regarding the identities of these blooms.

Table 2. Statistical summary (range, mean, and standard deviation) of in situ Chl-a and absorption properties for Florida Bay (1997-1998).

		Region				
	All data (n=30-48)	N-GFB (n=6-8)	S-GFB (n=7-10)	WFB (n=4-11)	NCFB (n=7-11)	SFB (n=5-8)
Chl-a ($mg\ m^{-3}$)	0.287-17.2, 3.87 ± 4.30	2.33-5.30, 4.08 ± 1.18	0.298-4.14, 1.29 ± 1.33	2.15-17.2, 6.86 ± 4.75	0.540-14.9, 4.38 ± 5.82	0.287-10.1, 2.10 ± 3.47
$a_{ph}(443)$ (m^{-1})	0.017-0.881, 0.169 ± 0.199	0.130-0.205, 0.169 ± 0.025	0.020-0.101, 0.050 ± 0.033	0.102-0.312, 0.174 ± 0.061	0.032-0.881, 0.251 ± 0.347	0.017-0.559, 0.173 ± 0.236
$a_{ph}(675)$ (m^{-1})	0.004-0.269, 0.068 ± 0.067	0.048-0.105, 0.076 ± 0.018	0.006-0.053, 0.020 ± 0.018	0.039-0.170, 0.096 ± 0.044	0.009-0.269, 0.077 ± 0.109	0.004-0.159, 0.049 ± 0.068
$a_{d}(443)$ (m^{-1})	0.007-0.617, 0.111 ± 0.131	0.038-0.348, 0.171 ± 0.092	0.007-0.039, 0.022 ± 0.012	0.061-0.617, 0.222 ± 0.187	0.022-0.181, 0.060 ± 0.046	0.011-0.068, 0.035 ± 0.024
$a_{CDOM}(443)$ (m^{-1})	0.136-0.745, 0.374 ± 0.158	0.136-0.337, 0.210 ± 0.070	0.194-0.381, 0.290 ± 0.071	0.186-0.658, 0.400 ± 0.200	0.386-0.745, 0.536 ± 0.142	0.384-0.472, 0.432 ± 0.034
$a_{tot}(443)$ (m^{-1})	0.284-1.61, 0.642 ± 0.342	0.473-0.733, 0.587 ± 0.115	0.284-0.425, 0.357 ± 0.048	0.441-1.20, 0.716 ± 0.338	0.470-1.611, 0.957 ± 0.480	0.431-1.066, 0.613 ± 0.239
$a^{*}_{ph}(443)$ ($m^{2}\ mg^{-1}$)	0.017-0.097, 0.044 ± 0.016	0.034-0.056, 0.043 ± 0.009	0.024-0.059, 0.038 ± 0.011	0.0.017-0.052, 0.030 ± 0.013	0.030-0.097, 0.055 ± 0.018	0.039-0.062, 0.053 ± 0.009
$a^{*}_{ph}(675)$ ($m^{2}\ mg^{-1}$)	0.010-0.022, 0.015 ± 0.003	0.016-0.022, 0.019 ± 0.002	0.012-0.016, 0.014 ± 0.001	0.010-0.019, 0.015 ± 0.003	0.011-0.020, 0.015 ± 0.003	0.010-0.016, 0.014 ± 0.003

Strong correlations were observed between Chl-a and phytoplankton absorption at 443nm and 675nm (r^2=0.90 and 0.97, respectively; n=42), and a moderate correlation was observed

between Chl-a and $a_d(443)$ (r^2=0.48, n=42) similar to relationships developed previously for global oceanic and other estuarine systems (Fig. 2 a-c) (Bricaud et al. 2004; Le et al. 2013). For bloom populations, the cyanobacteria bloom exhibited relatively high $a_{ph}(443)$ and low $a_d(443)$ compared to the diatom bloom. No correlation was found between Chl-a and $a_{CDOM}(443)$ (r^2=0.01, n=30) in contrast to a nearby river-dominated system (Bricaud et al. 2004; Le et al. 2013) (Fig. 2d).

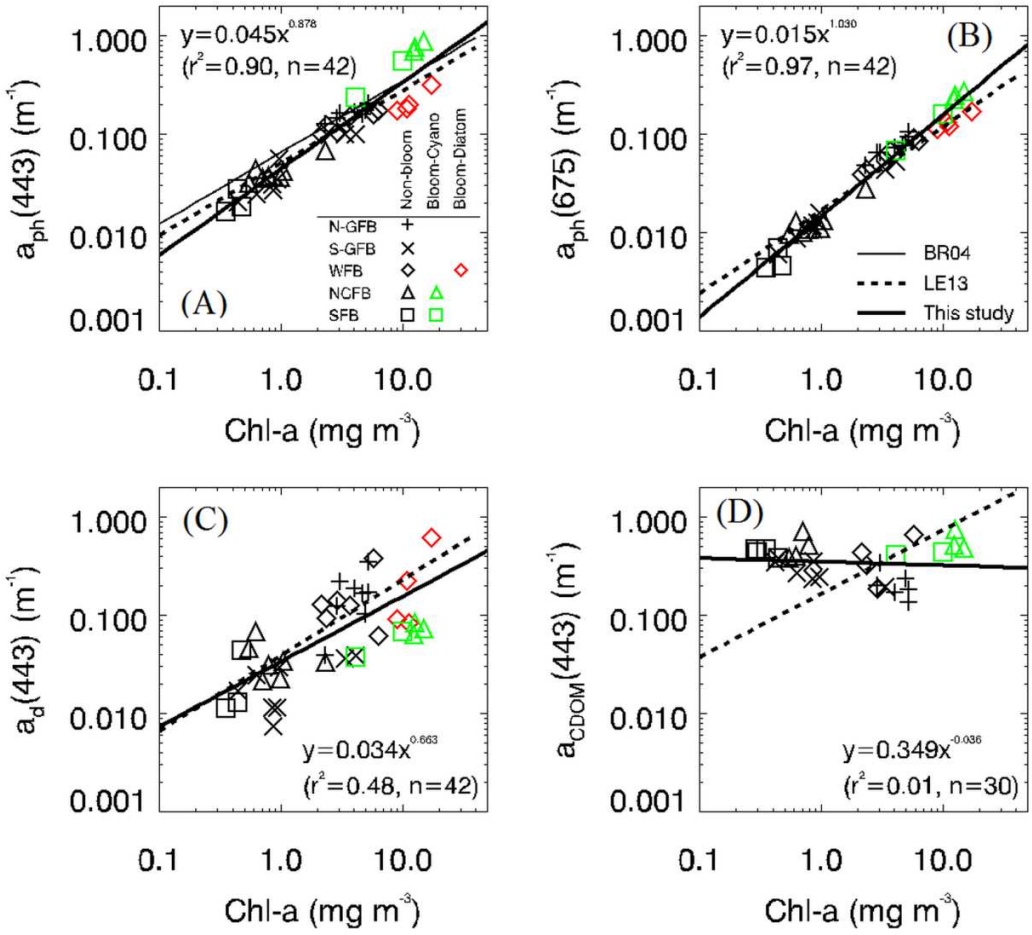

Figure 2. Relationships between in situ Chl-a and (A) $a_{ph}(443)$, (B) $a_{ph}(675)$, (C) $a_d(443)$, and (D) $a_{CDOM}(443)$ for Florida Bay and adjacent water bodies in 1997-1998. Symbols represent different regions: + = N-GFB, × = S-GFB, ◇ = WFB, △ = NCFB, and □ = SFB. Colors represent non-blooms (black) and blooms dominated by cyanobacteria (green) and diatoms (red). Thick solid lines represent best-fit power functions. Relationships developed previously for global oceanic (Bricaud et al., 2004) (BR04; thin solid line) and estuarine (Le et al., 2013) (LE13; dashed line) systems are shown for comparison.

In situ $R_{rs}(\lambda)$ showed large variability associated with changes in water column absorption and scattering properties and bottom reflectance characteristics (Fig. 3). Peak $R_{rs}(\lambda)$ occurred at green wavelengths (555-570nm) with magnitudes ranging widely from 0.006-0.064 sr^{-1}. Minor reflectance peaks at red wavelengths (670-680nm) caused by solar-stimulated chlorophyll-a fluorescence were highly pronounced mainly in diatom bloom populations (McKee et al. 2007; Morel and Prieur 1977). Relatively high $R_{rs}(555)$ (>0.025 sr^{-1}) was consistently observed in N-GFB and WFB where mean $a_d(443)$ was high (> 0.17 m^{-1}) and previous observations of increased scattering associated with high total suspended material (TSM) > 10 mg L^{-1} were reported (McPherson et al. 2011). Conversely, relatively low $R_{rs}(555)$ (<0.025 sr^{-1}) was found in seagrass-rich S-GFB where mean $a_d(443)$ was low (<0.03 m^{-1}) and previous observations of reduced scattering associated with low TSM (<5 mg L^{-1}) and increased bottom reflectance contributions were reported (Gao et al. 2007; McPherson et al. 2011).

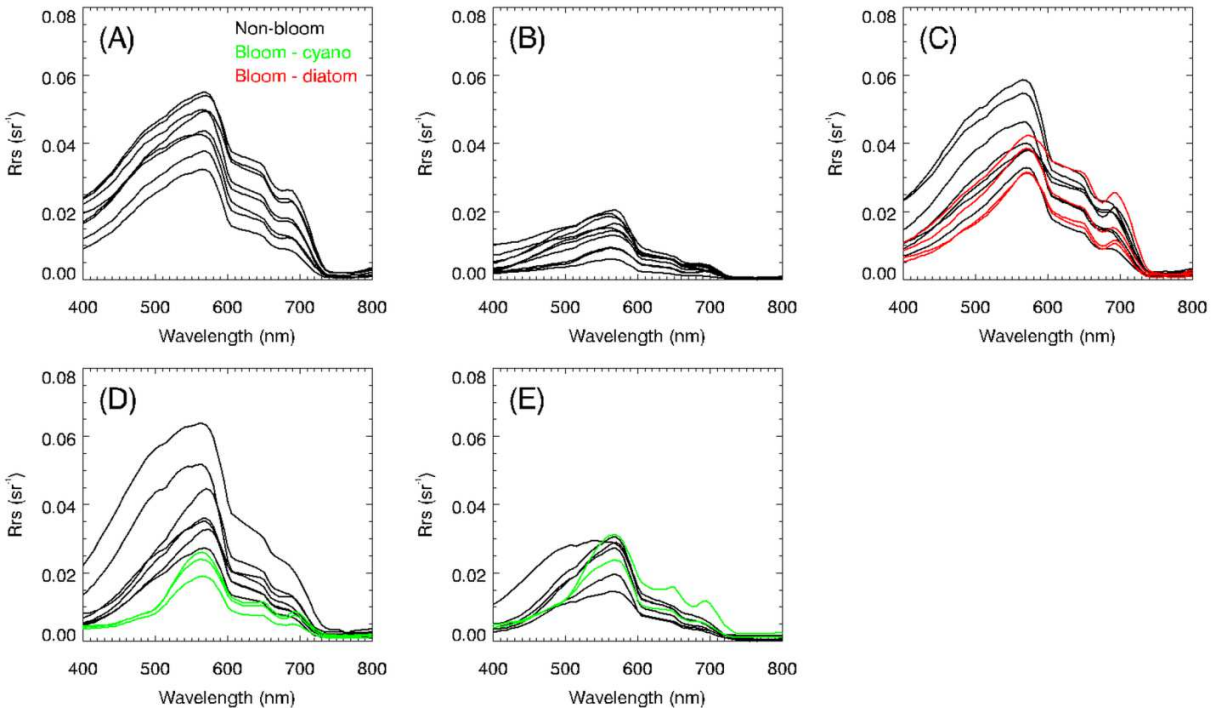

Figure 3. In situ remote sensing reflectance spectra (sr^{-1}) for Florida Bay and adjacent water bodies in 1997-1998 sorted by region: (A) N-GFB (B) S-GFB, (C) WFB, (D) NCFB, and (E)

SFB. Colors represent non-blooms (black) and blooms dominated by cyanobacteria (green) and diatoms (red).

$R_{rs}(\lambda)$ variability increased for NCFB and SFB, reflecting a wider range in absorption and scattering properties and bottom reflectance contributions in these regions. The cyanobacteria bloom exhibited moderate $R_{rs}(555)$ (~0.015-0.03 sr^{-1}) that were typically higher than seagrass-rich, non-bloom waters in S-GFB and lower than diatom bloom and turbid, non-bloom waters in N-GFB and WFB.

4.2 Spectral characteristics of Synechococcus blooms

Strong spectral agreement between mean $R_{rs}(\lambda)$ and 555nm-normalized $1/a_{tot}(\lambda)$ was observed for both the cyanobacteria (*Synechococcus*) and diatom bloom (Fig. 4a,b). This indicated that the spectral variability of $R_{rs}(\lambda)$ was largely driven by changes in absorption with the dominant absorbing constituent (phytoplankton, detritus, CDOM, or water) varying widely by wavelength and bloom type (Fig. 4c,d). Cyanobacteria bloom mean $R_{rs}(\lambda)$ exhibited unique

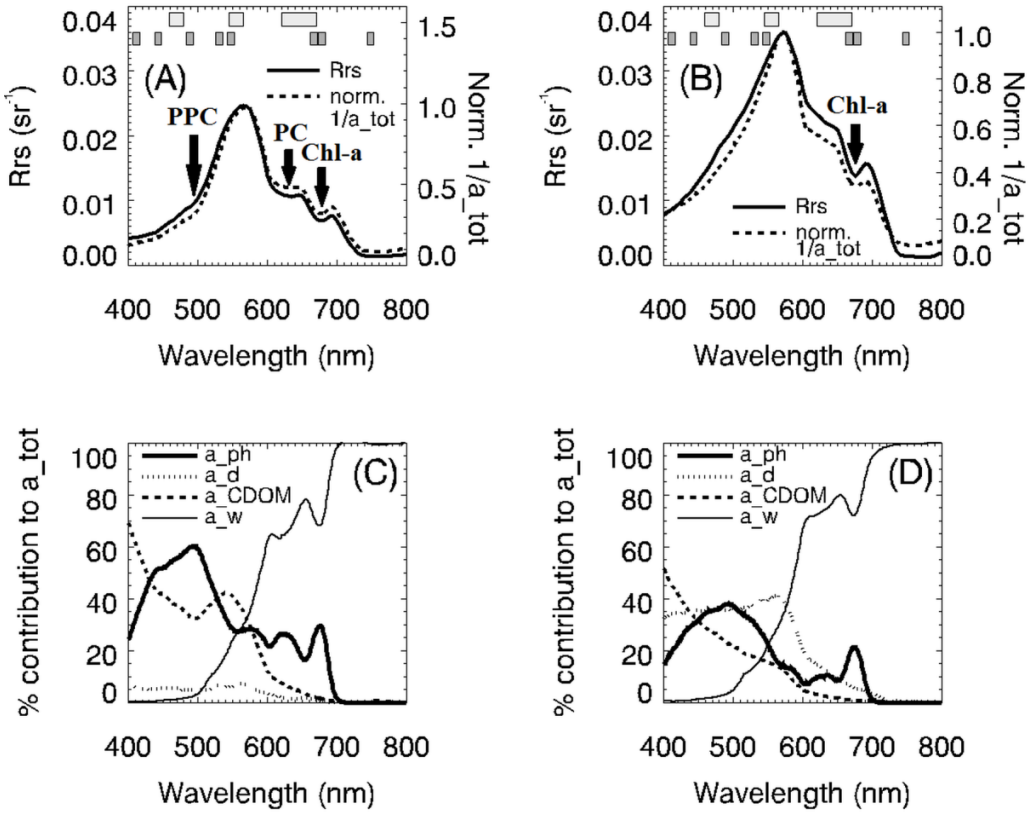

483

484 Figure 4. Mean in situ $R_{rs}(\lambda)$ (solid lines) and $1/a_{tot}(\lambda)$ normalized at 555nm (dashed lines) for the
485 1997 (A) cyanobacteria and (B) diatom blooms. Mean relative percent contribution (%) of
486 absorbing constituents [phytoplankton (solid thick lines), detritus (dotted lines), CDOM (dashed
487 lines), and water (solid thin lines)] to $a_{tot}(\lambda)$ for the 1997 (C) cyanobacteria and (D) diatom
488 blooms. Shaded regions in (A,B) show the location of MODIS ocean (dark gray) and land (light
489 gray) bands.
490

491 spectral features at around 490nm, 625nm, and 680nm (Fig. 4a) similar to freshwater *Microcystis*

492 blooms (Moore et al. 2017). These features occurred in spectral regions where enhanced $a^*_{ph}(\lambda)$

493 (Fig. 5) and low $a_d(\lambda)$ contributions (<5%) led to phytoplankton contributing strongly to $a_{tot}(\lambda)$

494 (~25-60%) (Fig. 4c).

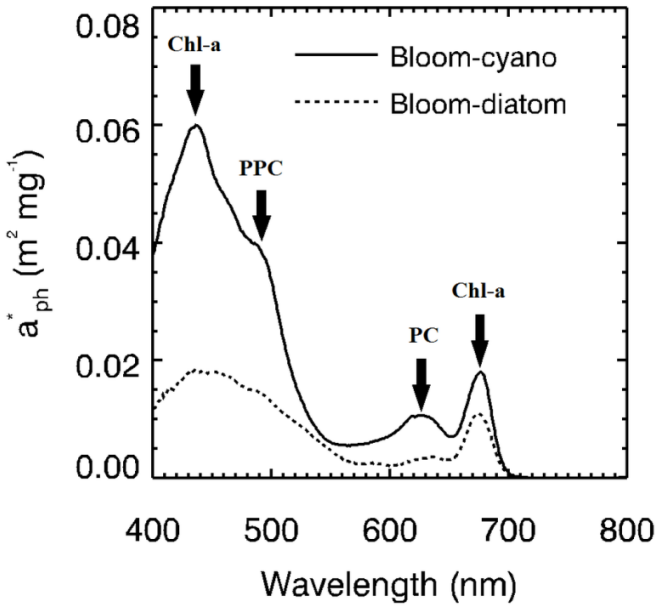

Figure 5. Mean in situ chlorophyll-specific phytoplankton absorption spectra, $a^*_{ph}(\lambda)$, for the 1997 cyanobacteria (solid line) and diatom (dashed line) blooms.

The sharp negative inflection in reflectance at 490nm was caused by strong carotenoid absorption and weak pigment packaging based on the relatively high $a^*_{ph}(490)$ (~0.04 m^2 mg^{-1}) (Fig. 5). Pigment packaging refers to the way pigments are "packaged" within cells and increases with increasing cell size and intracellular pigment concentration (Morel and Bricaud 1981). In contrast, diatom bloom mean $R_{rs}(\lambda)$ was nearly spectrally flat between 440-550nm (Fig. 4b) caused by higher $a_d(\lambda)$ contributions to $a_{tot}(\lambda)$ (~35-40%) (Fig. 4d) and lower (<0.02 m^2 mg^{-1}) and spectrally featureless $a^*_{ph}(\lambda)$ (Fig. 5). $R_{rs}(\lambda)$ spectral curvature between 440-550nm for non-bloom waters was also mainly flat or convex for a large range of absorption and scattering properties and bottom reflectance contributions (Fig. 3).

The reflectance trough at 625nm observed in the cyanobacteria bloom mean $R_{rs}(\lambda)$ (Fig. 4a) can be attributed to PC absorption (Fig. 5). The absence of this feature in $R_{rs}(\lambda)$ for the diatom bloom and non-bloom waters (Figs. 3, 4b) suggests that PC detection algorithms utilizing the MERIS and OLCI 620nm ocean bands (Qi et al. 2014; Schalles and Yacobi 2000; Simis et al.

512 2005) may perform well in this region. Unfortunately, however, the performance of such
513 algorithms could not be tested here because PC concentrations were not available. The location
514 of the red reflectance trough/peak for the cyanobacteria bloom (680/695nm) was also unique as it
515 was red-shifted ~5nm compared to the diatom bloom (675/690nm) (Fig. 4a,b). It is this dip in
516 reflectance at ~680nm that forms the basis for the MERIS and MODIS CI algorithms (Wynne et
517 al. 2013; Wynne et al. 2008).

518 In summary, these field-based measurements indicate that positive CI_{MODIS} and a
519 negative spectral shape around 488nm, SS(488), determined with Equation (1) using MODIS
520 bands ($\lambda^- = 443$nm, $\lambda = 488$nm, and $\lambda^+ = 547$nm) may be unique to cyanobacteria blooms
521 dominated by *Synechococcus* in Florida Bay. Figure 6 shows the relationship between CI_{MODIS}
522 and SS(488) derived from in situ $R_{rs}(\lambda)$. Indeed, the cyanobacteria bloom exhibited mostly
523 positive CI_{MODIS} and negative SS(488), allowing for this bloom to largely be differentiated from
524 diatom bloom and non-bloom waters. Where cyanobacteria bloom CI_{MODIS} was negative, Chl-a
525 was <10 mg m^{-3}, indicating a weaker bloom with mixed phytoplankton assemblages (Phlips and
526 Badylak 1996; Phlips et al. 1999).
527
528 ***4.3 Algorithm development and validation***
529 Following the spectral analysis results above, the relationship between CI_{MODIS} and
530 SS(488) derived from MODIS $R_{rc}(\lambda)$ for the 2002-2012 match-up data set showed similar
531 patterns compared to the 1997-1998 in situ data (Fig. 7a). Cyanobacteria blooms exhibited

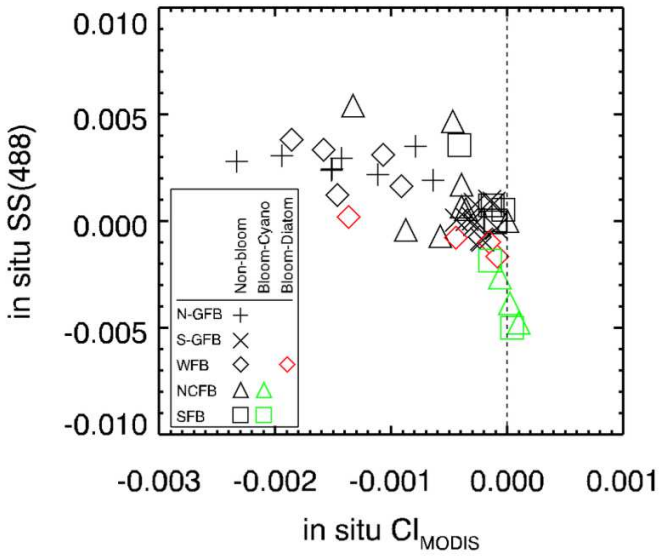

532

533 Figure 6. Relationship between CI_{MODIS} and SS(488) derived from in situ $R_{rs}(\lambda)$ for Florida Bay
534 and adjacent water bodies in 1997-1998. Symbols represent different regions: + = N-GFB, × =
535 S-GFB, ◇ = WFB, △ = NCFB, and □ = SFB. Colors represent non-blooms (black) and blooms
536 dominated by cyanobacteria (green) and diatoms (red). The vertical dashed line represents where
537 $CI_{MODIS} = 0$ (Wynne et al., 2013).
538

539 mostly positive CI_{MODIS} and negative SS(488) compared to 'other' (non-PC containing) blooms
540 and non-bloom waters. Using the original classification criteria developed for freshwater
541 cyanobacteria blooms ($CI_{MODIS} > 0$) (or 'original CI approach') (Wynne et al. 2013), the FM was
542 0.66 (Table 3). Although sensitivity was relatively high (0.84), precision was low (0.63) with
543 2.5% false positives. Optimizing the CI_{MODIS} threshold whereby cyanobacteria blooms were
544 positively classified when $CI_{MODIS} > 0.0003$ increased the FM to 0.75. Precision also increased
545 to 0.78 and false positives decreased to 0.9%, but sensitivity decreased to 0.66 as the percentage
546 of false negatives doubled (15.6% to 34.4%).

547 Implementing dual classification criteria whereby cyanobacteria blooms were flagged
548 positive when $CI_{MODIS} > 0$ and SS(488) < -0.0055 led to maximal FM (0.88). Using this modified
549 CI approach, 75% of cyanobacteria blooms were classified accurately and only two false positive
550 classifications occurred for stations located at bloom edges during periods of confirmed

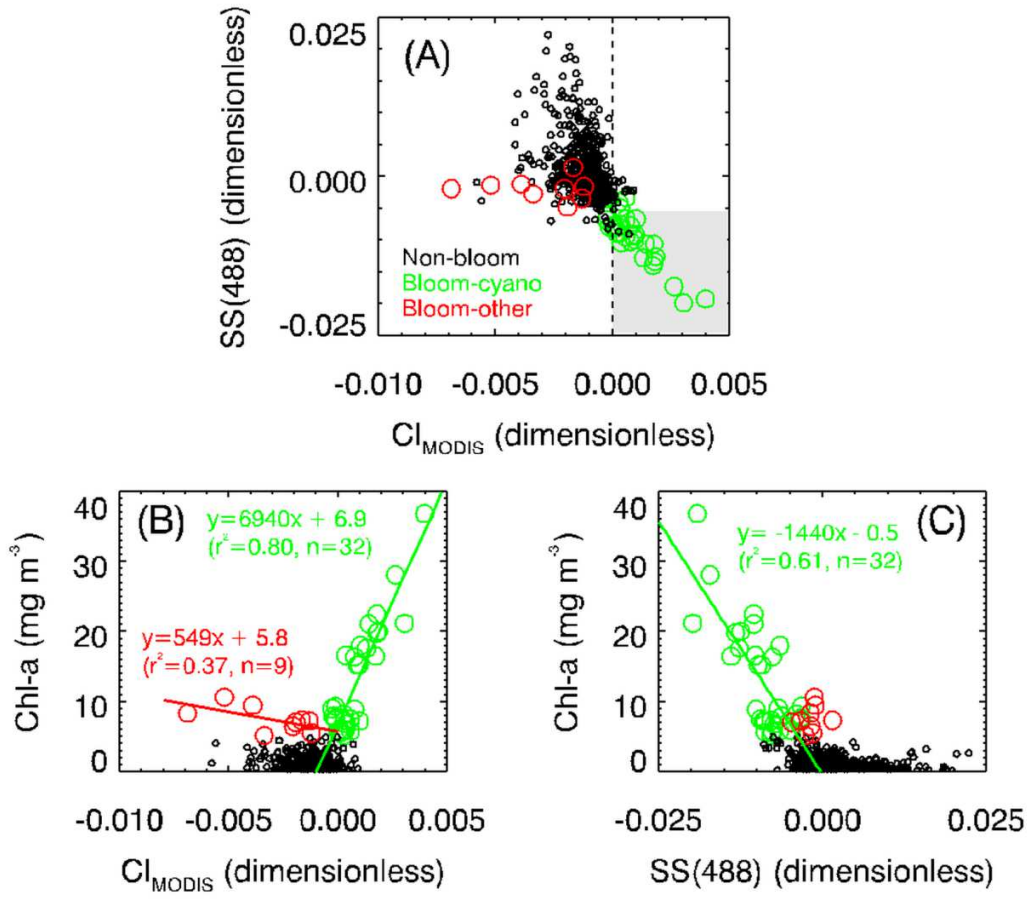

551

552 Figure 7. Relationships between (A) CI_{MODIS} and SS(488), (B) CI_{MODIS} and in situ Chl-a (mg m^{-3}), and (C) SS(488) and in situ Chl-a (mg m^{-3}). CI_{MODIS} and SS(488) were derived from MODIS/Aqua $R_{rc}(\lambda)$ (dimensionless) for Florida Bay and adjacent waters (NOAA; 2002-2012). Colors represent non-blooms (black), cyanobacteria blooms (green), and 'other' blooms (red). The vertical dashed line in (A) represents where $CI_{MODIS} = 0$ (Wynne et al., 2013) and the gray shaded area represents where $CI_{MODIS} > 0$ and SS(488) < -0.0055.

558

559 cyanobacteria blooms (Evans et al. 2006; Glibert et al. 2004). Also, 100% of 'other' blooms

560 exhibited negative CI_{MODIS}, illustrating that this technique was capable of discriminating

561 cyanobacteria blooms from other bloom types. For cyanobacteria blooms with Chl-a up to 37 mg

562 m^{-3}, a strong positive correlation was observed between in situ Chl-a and CI_{MODIS} (r^2=0.80,

563 n=32) compared to a slightly weaker negative correlation between in situ Chl-a and SS(488)

564 (r^2=0.61, n=32) (Fig. 7b,c). This indicated that cyanobacterial Chl-a derived from CI_{MODIS}, Chl_{CI},

565 can accurately be determined for pixels positively flagged as cyanobacteria blooms.

566

567 Table 3. Pixel-based statistics determined using confusion matrixes for comparing various
568 cyanobacteria bloom detection approaches.

Technique	Threshold(s)	A (cb-CB)	B (cb-NCB)	C (ncb-CB)	D (ncb-NCB)	FM	Sensitivity A/(A+B)	Precision A/(A+C)	False neg. % B/(A+B)	False pos. % C/(C+D)
Original CI	$CI_{MODIS} > 0$	27	5	16	634	0.66	0.84	0.63	15.6	2.5
Optimized CI	$CI_{MODIS} > 0.0003$	21	11	6	644	0.75	0.66	0.78	34.4	0.9
Modified CI	$CI_{MODIS} > 0$, SS(488) < -0.0055	24	8	2	648	0.88	0.75	0.92	25.0	0.3

569

570 Performance of the original CI approach and new modified CI approach was evaluated
571 next using imaged-based analysis to assess how these methods work in areas where in situ data
572 for algorithm development was not available. Based on shipboard Chl-a and PC fluorescence
573 collected on 28-29 September 2016 (Fig. 8a,b) and visual interpretation of a MODIS/Terra 'true-
574 color' RGB-composite image from 28 September 2016 (Fig. 8c), four distinct optical water types
575 were identified:

576 (1) A cyanobacteria bloom, located in NCFB and SFB, exhibited high Chl-a (7-42 mg m^{-3}) and
577 high PC fluorescence (>0.5 RFU), appearing olive-green in the MODIS RGB image.
578 (2) A spatially separate 'other' bloom with moderately high Chl-a (7-11 mg m^{-3}) and low PC
579 fluorescence (<0.5 RFU) occurred in northern WFB, appearing chalky tan in the MODIS
580 RGB image.
581 (3) Seagrass-rich, non-bloom waters with low Chl-a (<1 mg m^{-3}) were observed in southern
582 WFB, appearing dark in the MODIS RGB image.

583 (4) Turbid, non-bloom waters in NEFB and northern WFB also exhibited relatively low Chl-a

584 (0.5 and 4 mg m^{-3}, respectively), but appeared chalky blue-green in the MODIS RGB image.

585

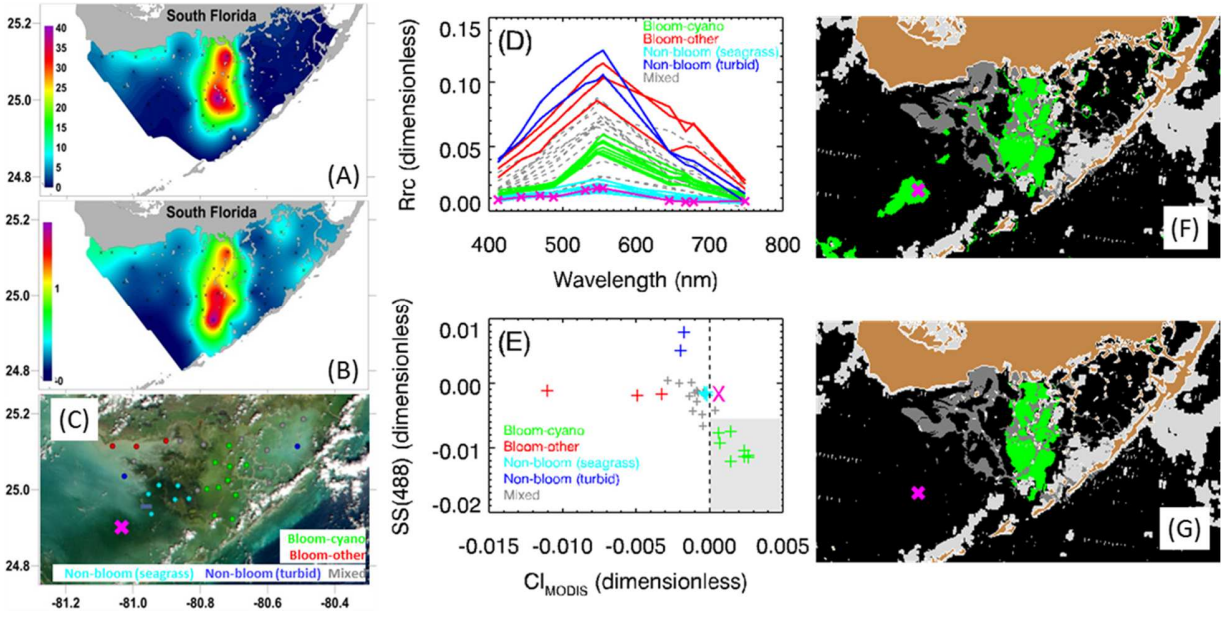

586

587 Figure 8. In situ (A) Chl-a (mg m^{-3}) and (B) phycocyanin fluorescence (relative fluorescence
588 units) collected on 28-29 September 2016. (C) MODIS/Terra RGB-composite image (28
589 September 2016) with station locations representing four distinct optical water types and mixed
590 water types overlaid. The magenta 'X' marks a seagrass-rich, non-bloom location in S-GFB
591 where false positive flagging of cyanobacteria blooms occurred when pixels were classified
592 based on $CI_{MODIS} > 0$ (original CI approach; Wynne et al., 2013). (D) MODIS/Terra $R_{rc}(\lambda)$
593 (dimensionless) and (E) relationship between CI_{MODIS} (dimensionless) and SS(488)
594 (dimensionless) sorted by optical water type. The vertical dashed line in (E) represents where
595 $CI_{MODIS} = 0$ and the gray shaded area represents where $CI_{MODIS} > 0$ and $SS(488) < -0.0055$. (F-G)
596 Classified MODIS/Terra image (28 September 2016) showing positively flagged cyanobacteria
597 bloom pixels (green) classified according to (F) $CI_{MODIS} > 0$ (original CI approach; Wynne et al.,
598 2013) and (G) $CI_{MODIS} > 0$ and $SS(488) < -0.0055$ (modified CI approach; this study). Non-
599 cyanobacteria bloom pixels are shaded black, clouds are light gray, mud banks are dark gray, and
600 land is tan.
601

602 The relative magnitudes and spectral shapes of MODIS $R_{rc}(\lambda)$ for the 2016 cyanobacteria

603 bloom (Fig. 8d) closely resembled the in situ $R_{rs}(\lambda)$ for the 1997 cyanobacteria bloom (Fig. 3).

604 MODIS $R_{rc}(555)$ was higher compared to seagrass-rich, non-bloom waters and lower compared

605 to 'other' bloom and turbid, non-bloom waters. A sharp negative inflection in reflectance at

606 490nm was clearly evident for the cyanobacteria bloom and absent for all other optical water
607 types. Also, red reflectance peaks attributed to solar-stimulated chlorophyll-a fluorescence were
608 highly prominent for the 'other' bloom, but largely absent for cyanobacteria bloom and non-
609 bloom waters.

610 The original CI approach only worked partially in this region. Although 100% of
611 cyanobacteria bloom stations exhibited $CI_{MODIS} > 0$ and therefore were accurately classified (Fig.
612 8e) and the areal extent of the cyanobacteria bloom was successfully captured by MODIS (Fig.
613 8f), several regions, mainly in seagrass-rich waters that appear dark in the MODIS RGB image,
614 were also positively flagged as cyanobacteria blooms. The magenta X in Figure 8c depicts a
615 shallow (<2 m) site in S-GFB overlying dense *Syringonium* beds where CI_{MODIS} was positive, yet
616 shipboard data collected a week prior confirmed the absence of any bloom (unpublished data,
617 NOAA-AOML). MODIS $R_{rc}(\lambda)$ at this site was low (< 0.02) and tailed up slightly at 748nm (Fig.
618 8d), explaining why CI_{MODIS} was positive. Application of the modified CI approach successfully
619 eliminated the false positive flags in this region and also in shallow (<1 m) seagrass-rich waters
620 adjacent to mud banks without impacting classification accuracies for the true cyanobacteria
621 bloom (Fig. 8g). Therefore, modifying the original CI approach to include SS(488) allowed
622 weaker cyanobacteria blooms with Chl-a < 10 mg m^{-3} to be differentiated from seagrass-rich,
623 non-bloom waters.

624 Algorithm performance was validated using cyanobacteria cell abundances measured
625 with flow cytometry. Figure 9 shows a series of MODIS/Aqua Chl_{CI} images for the late-2013
626 cyanobacteria bloom event. This bloom originated in NCFB in early-September and shifted
627 slowly southward and strengthened over the next month. On 10 October, Chl_{CI} peaked at 46 mg
628 m^{-3} in SFB where high total cyanobacteria abundances (~12-16 x 10^6 cells ml^{-1}) measured a day

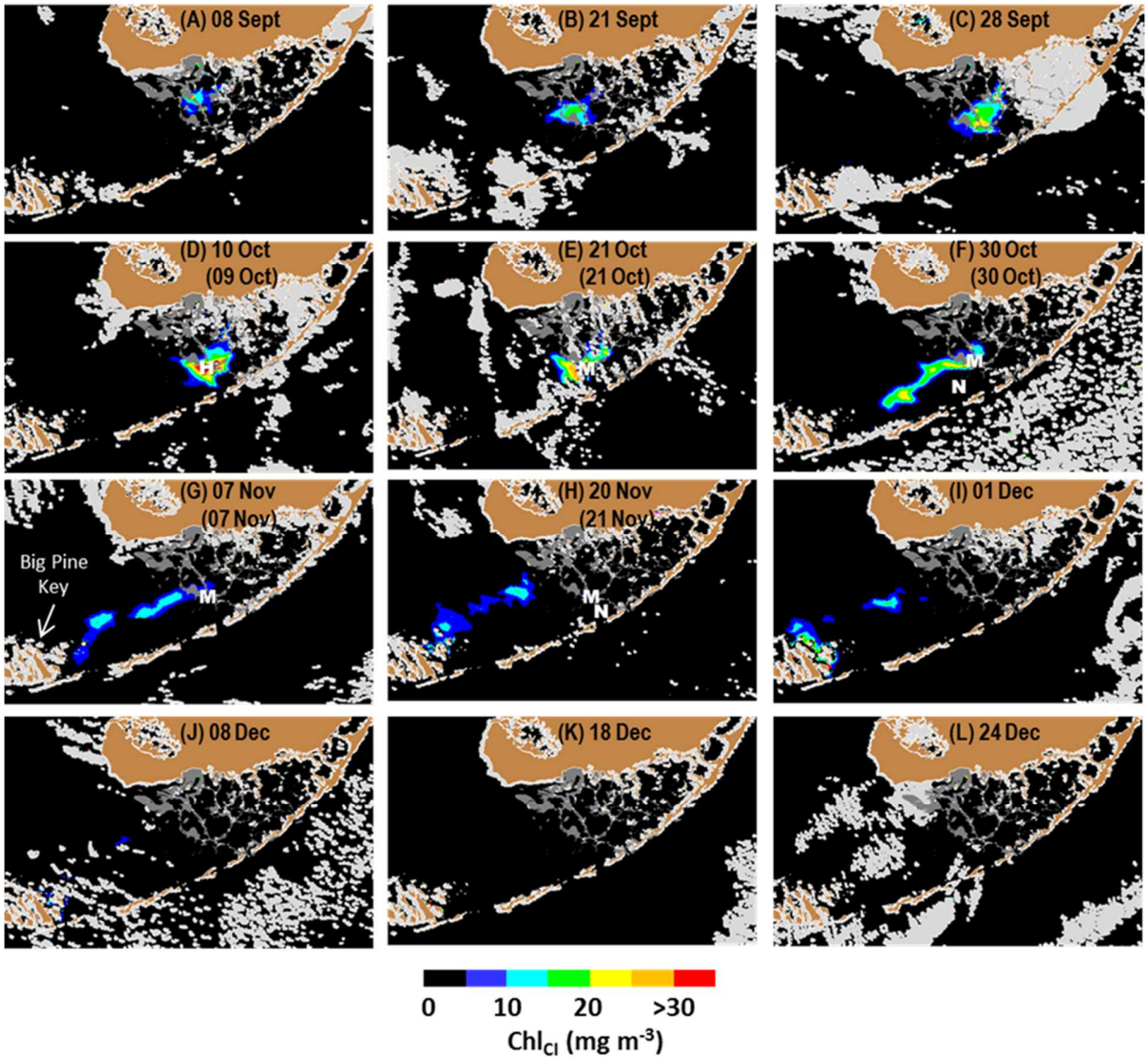

Figure 9. MODIS/Aqua Chl_{CI} (mg m^{-3}) image series showing bloom transport in late-2013. Chl_{CI} was derived using the modified CI approach. The first date is when the image was collected. The second date (in parenthesis) indicates the in situ sampling date. Letters overlaid on the images are water sample analysis results from FWC-FWRI indicating different levels of total cyanobacteria cellular abundances (cells ml^{-1}): H= 'high' bloom (>10^7), M= 'medium' bloom (10^6-10^7), L= 'low' bloom (0.45 x 10^6-10^6), and N= 'non-bloom' (<0.45 x 10^6). Non-cyanobacteria bloom pixels are shaded black, clouds are light gray, mud banks are dark gray, and land is tan.

prior were observed. Following the passage of a strong cold front on October 24th, the bloom spread toward the southwest and into S-GFB. On 7 November, a weakened bloom with Chl_{CI} <16 mg m^{-3} appeared as a narrow (~4 km) filament extending ~50 km from WFB to Big Pine

642 Key, FL. Medium cyanobacteria abundance (~5 x 10^6 cells ml^{-1}) measured that same day was
643 associated with this feature. This bloom persisted for approximately three months, terminating in
644 early-December.
645
646 ***4.4 MODIS and MERIS comparison***
647 A comparison of same-day MODIS and MERIS imagery collected on 23 November 2006
648 during a known *Synechococcus* bloom (Berry et al. 2015) revealed similarities in high biomass
649 (>20 mg m^{-3}) bloom patterns for MODIS Chl_{CI} determined with the modified CI approach (Fig.
650 10c) and MERIS Chl_MPH for pixels flagged positive for cyanobacteria using SICF, SIPF, and
651 BAIR (Matthews et al. 2012; Matthews and Odermatt 2015) (Fig. 10f). This suggests that after
652 local tuning of the MPH algorithm parameterization to capture weaker blooms (<20 mg m^{-3}),
653 MERIS (and therefore OLCI because these sensors basically have the same design) is likely to
654 yield consistent results as from MODIS.
655 This comparison also further highlights the need for inclusion of spectral shapes in
656 addition to those based on red and near-IR wavebands for classifying blooms in areas prone to
657 strong bottom reflectance contributions. False positive classifications were observed in shallow,
658 seagrass-rich, non-bloom waters west of the bloom (circled regions in Figure 10) for both
659 MODIS when using the original CI approach (Wynne et al. 2013) (Fig. 10b) and MERIS
660 Chl_MPH when the additional cyanobacteria flagging variables were not considered (Fig. 10e).
661 For MERIS Chl_MPH with no cyanobacteria flagging, false positive cyanobacteria detections
662 were also observed in traditionally low biomass oligotrophic and mesotrophic waters located
663 outside of Florida Bay. Testing for the presence of a 709nm peak position using the BAIR
664 variable effectively eliminated these false detections (Matthews and Odermatt 2015).

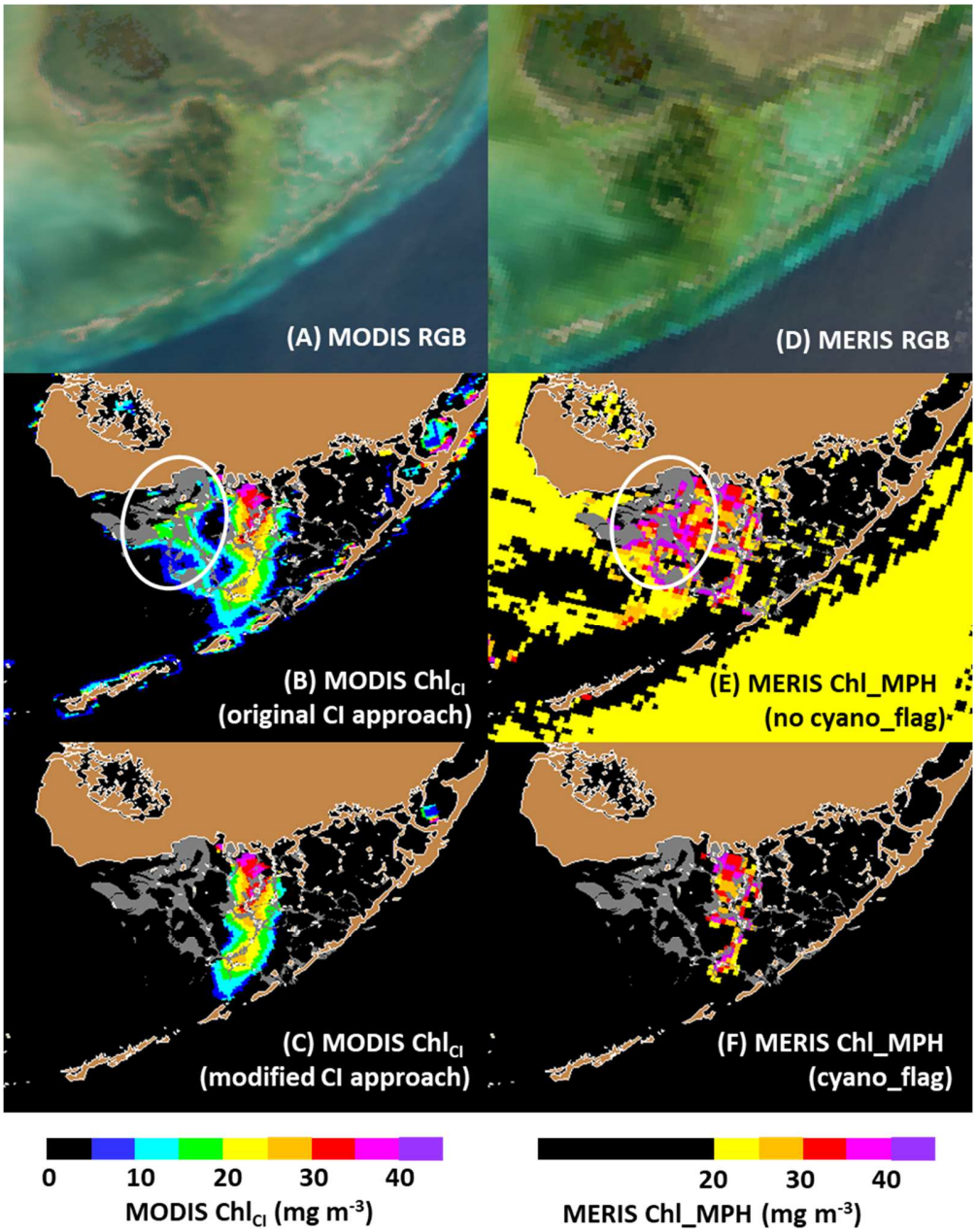

Figure 10. Comparison of MODIS and MERIS cyanobacteria bloom detection techniques for imagery collected on the same day. MODIS/Aqua (A) RGB, (B) Chl_{CI} (original CI approach), and (C) Chl_{CI} (modified CI approach) for 23 November 2006 (18:10 UTC). MERIS (D) RGB, (E) Chl_MPH (no cyano_flag), and (F) Chl_MPH (cyano_flag) for 23 November 2006 (15:36 UTC). MERIS Chl_MPH was determined according to Matthews et al. (2012; 2015). The cyano_flag provides a means for discriminating cyanobacteria blooms from eukaryotic-dominated blooms and employs various spectral shapes (SICF, SIPF, and BAIR). The circled areas depict seagrass-rich, non-bloom waters west of the bloom that are false positively flagged as cyanobacteria blooms for MODIS Chl_{CI} when using the original CI approach (B) and MERIS Chl_MPH when the cyanobacteria flags are not applied (E).

677 ***4.5 Algorithm sensitivity to variable observing conditions***

678 Although it has been shown that baseline subtraction algorithms are mostly immune to
679 variable observing conditions when using $R_{rc}(\lambda)$ at red and NIR wavebands (e.g., CI_{MODIS}), the
680 influence of changing aerosols on SS(488), which involves blue-green wavebands (443nm,
681 488nm) where aerosol contributions may be more important, has yet to be determined. Hence,
682 following the approach of Hu (2009) for floating macroalgae and Qi et al. (2014) for floating
683 cyanobacteria, model simulations were conducted to evaluate whether there is a tight relationship
684 between SS(488) derived from in situ $R_{rs}(\lambda)$ and SS(488) derived from MODIS $R_{rc}(\lambda)$ for a
685 variety of conditions.

686 Based on radiative transfer theory and assuming a non-coupling ocean-atmosphere
687 system and the absence of whitecaps and sun glint, $R_{rc}(\lambda)$ can be expressed as (Hu, 2009)

688 $$R_{rc}(\lambda) = \rho_t(\lambda) - \rho_r(\lambda) = \rho_a(\lambda) + \pi\, t(\lambda)\, t_0(\lambda)\, R_{rs}(\lambda) \quad (3)$$

689 where ρ_t is the top-of-atmosphere (TOA) reflectance, ρ_r is the reflectance due to Rayleigh
690 scattering, ρ_a is the reflectance due to aerosol scattering and aerosol-Rayleigh interactions, $t(\lambda)$ is
691 the diffuse transmittance from the ocean to the satellite, and $t_0(\lambda)$ is the diffuse transmittance
692 from the sun to the ocean. Two sensor viewing geometries were considered: "scene center" near
693 satellite nadir (satellite zenith $\theta = 4^o$) and "scene edge" near the satellite's scan edge ($\theta = 57^o$).
694 For each viewing geometry, $\rho_a(\lambda)$ was estimated using aerosol lookup tables for MODIS
695 (available from SeaDAS data processing software) for two different aerosol types (M90 =
696 maritime aerosol with 90% relative humidity and C50 = coastal aerosol with 50% relative
697 humidity) and aerosol optical thicknesses ($\tau869 = 0.04$ (or "min"; representing a clear sky) and
698 0.3 (or "max"; representing a hazy atmosphere). Note that Level-1 MODIS data with $\tau869 > 0.3$
699 are masked with SeaDAS without being processed.

For the eight individual scenarios tested, relationships between SS(488) derived from in situ $R_{rs}(\lambda)$ and SS(488) derived from simulated MODIS $R_{rc}(\lambda)$ showed strong correlations (r^2>0.98, n=47) (Fig. 11a,b). Most importantly, the relationship between the two SS(488) (from $R_{rs}(\lambda)$ and $R_{rc}(\lambda)$, respectively) appeared to be stable. Indeed, combining all of these scenarios

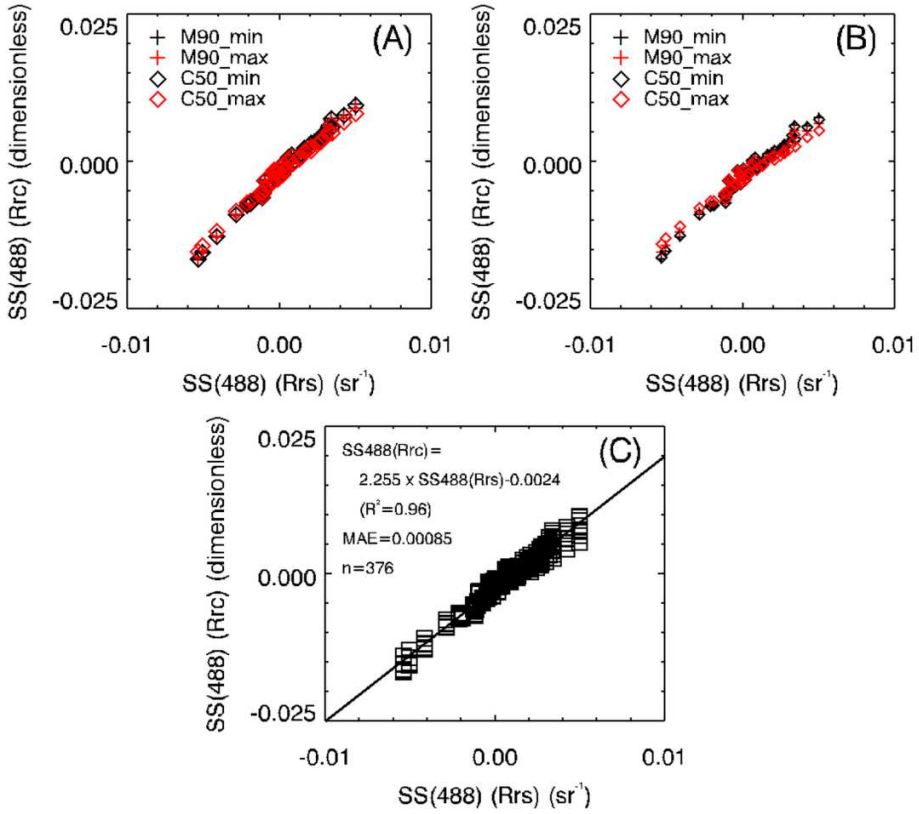

Figure 11. Relationships between SS(488) derived from in situ $R_{rs}(\lambda)$ (sr^{-1}) and SS(488) derived from MODIS $R_{rc}(\lambda)$ (dimensionless) simulated based on radiative transfer theory (Eq. 3). Simulations were conducted for sensor viewing geometries at (A) scene center (θ=4°) and (B) scene edge (θ=57°) and for variable aerosol types (+: M90, ◇: C50) and aerosol optical thicknesses (black='min' (τ869=0.04) and red='max' (τ869=0.3)). The results from all simulations combined are shown in (C). The solid line represents the best-fit linear function. Uncertainty based on the mean absolute error (MAE) is also provided.

together continued to yield a strong correlation expressed as SS(488) (R_{rc}) = 2.255*SS(488) (R_{rs}) – 0.0024 (r^2=0.96, n=376) (Fig. 11c). The uncertainty in SS(488) (R_{rc}) as determined with the mean absolute error (MAE) was 8.5 x 10^{-4}. Given that the modified CI approach utilizes a

constant SS(488) threshold (-0.0055) for identifying cyanobacteria blooms (Fig. 7a) and the estimated uncertainty of SS(488) (Rrc) was only 15% of this threshold, this indicated that this uncertainty will minimally impact classification accuracies.

The tolerance of the modified CI approach to variable sensor viewing geometries was further confirmed with image analysis. Figure 12 shows the MODIS/Aqua imagery collected on 10 October 2013 (θ=21.4°) and 11 October 2013 (θ=64.1°). Even though the viewing angle on 11 October exceeded the "large-angle" threshold of 60° from the SeaDAS processing (l2_flags), the cyanobacterial bloom appeared to be the same on both dates in the Chl_{CI} imagery (Fig. 12b,d), with their histograms showing very similar Chl_{CI} distributions (Fig. 12e).

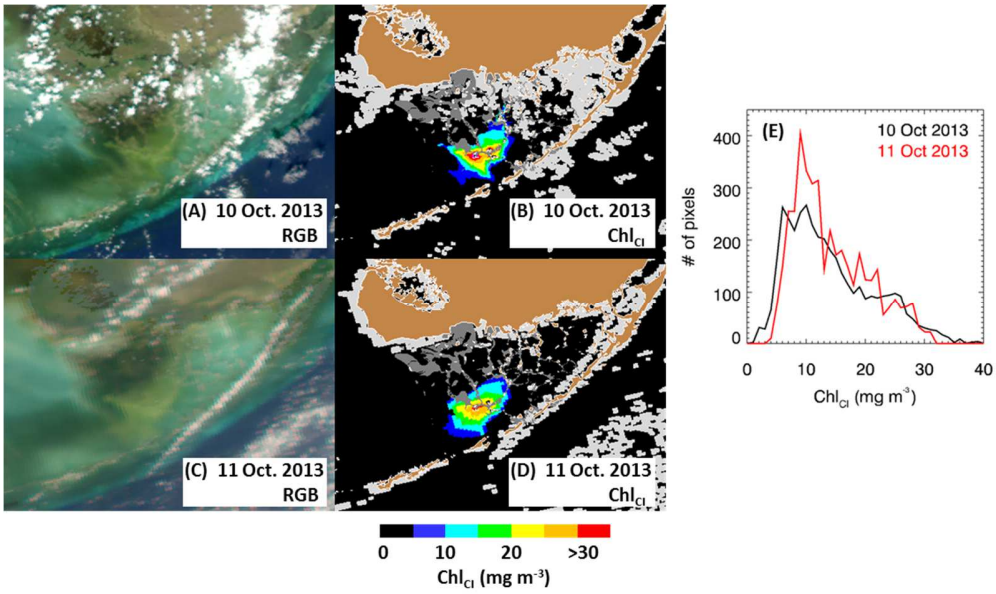

Figure 12. Example showing how the modified CI approach is insensitive to variable sensor viewing geometry. (a) and (b) show MODIS/Aqua RGB-composite imagery and Chl_{CI} (mg m^{-3}) on 10 October 2013 (θ=21.4°). (c) and (d) show MODIS/Aqua RGB-composite imagery and Chl_{CI} (mg m^{-3}) on 11 October 2013 (θ=64.1°). The histograms in (e) show Chl_{CI} distribution statistics on 10 October 2013 (black) and 11 October 2013 (red) for areas positively classified as cyanobacteria blooms.

4.6 Application to the 2005-2008 bloom event

Figure 13 shows a time-series of in situ Chl-a and daily MODIS/Aqua Chl_{CI} for select stations located throughout Florida Bay and adjacent water bodies during the widespread and persistent 2005-2008 cyanobacteria bloom event. Chl_{CI} was set equal to zero for pixels flagged

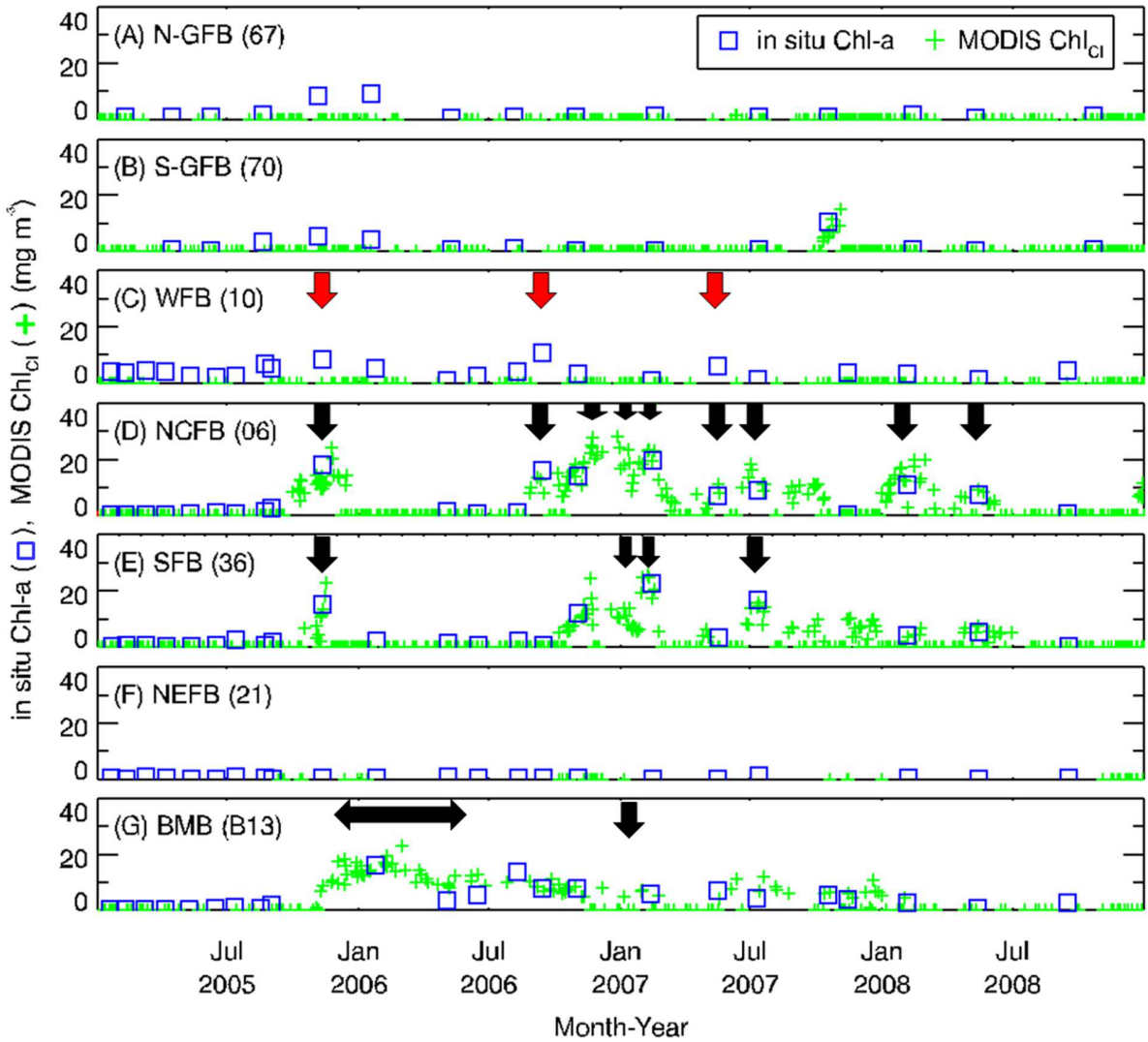

Figure 13. In situ Chl-a (mg m^{-3}) (○) and daily MODIS/Aqua Chl_{CI} (mg m^{-3}) (+) in (A) N-GFB, (B) S-GFB, (C) WFB, (D) NCFB, (E) SFB, (F) NEFB, and (G) BMB for the 2005-2008 cyanobacteria bloom event. NOAA station locations (in parenthesis) are shown in Figure 1a. Chl_{CI} was set equal to zero for non-cyanobacteria bloom pixels. Black and red arrows indicate confirmed cyanobacteria and 'other' blooms, respectively. Confirmation was based on field measurements presented in this study and from previous studies (Berry et al., 2015; Garner and McCarthy, 2009; Glibert et al., 2009).

746

747 as non-cyanobacteria blooms. Based on the new approach, cyanobacteria blooms were never
748 observed at the stations located in N-GFB, WFB, and NEFB and were only rarely observed in S-
749 GFB. Instead, 'other' blooms with in situ Chl-a > 5 mg m^{-3} and $Chl_{CI} = 0$ occurred periodically
750 in N-GFB and WFB consistent with historical patterns (Jurado et al. 2007).

751 Cyanobacteria blooms in NCFB and SFB were observed throughout much of 2005-2008
752 and exhibited maximal Chl_{CI} (41 mg m^{-3}) that was nearly twice as high compared to a spatially
753 distinct bloom in BMB (23 mg m^{-3}). Blooms in both regions were first observed in late-2005
754 during an active storm season when Hurricanes Katrina (August), Rita (September), and Wilma
755 (October) passed South Florida, causing nutrient concentrations to increase in South Florida
756 estuaries (Glibert et al. 2009). Additional nutrients released directly into BMB as part of a local
757 road-widening project likely contributed to the persistence of this bloom throughout much of
758 2006.

759

760 **5. Discussion**

761 ***5.1 Why the new approach works***

762 The original CI approach was developed for detecting high-biomass (Chl-a ~20-100 mg
763 m^{-3}) freshwater cyanobacteria blooms that often form vast dense surface mats (Wynne et al.
764 2013; Wynne et al. 2008). Over the past decade, this approach has shown broad applicability
765 across multiple sensors (MERIS, MODIS), bloom-forming genera (*Microcystis*, *Planktothrix*,
766 *Nodularia*), and water bodies (freshwater, brackish) (Lunetta et al. 2015; Moradi 2014;
767 Tomlinson et al. 2016; Zhang et al. 2017). However, when applied to marine picocyanobacteria
768 blooms dominated by *Synechococcus* in an optically complex, lagoonal estuary prone to strong

769 bottom reflectance contributions (Florida Bay), false positive detections were commonly
770 observed in non-bloom areas overlying dense seagrass beds. Modification of this approach to
771 include SS(488) was shown to effectively remove these false positive detections, leading to
772 successful detection and quantification of blooms for Chl_{CI} ~5-40 mg m^{-3}.
773 While CI is of empirical nature, it is based on fundamental optical properties of
774 cyanobacteria. Positive CI in cyanobacteria blooms has been attributed to strong chlorophyll-a
775 absorption at ~680nm, low chlorophyll-a fluorescence, and high scattering (Wynne et al. 2013;
776 Wynne et al. 2008). A major driving force for CI is that chlorophyll-a in cyanobacteria is mostly
777 contained within the non-fluorescing Photosystem I (Johnsen and Sakshaug 1996). This causes
778 the red absorption peak in cyanobacteria (~680nm) to be red-shifted compared to eukaryotic
779 algae (~676nm) (Hoepffner and Sathyendranath 1991; Wojtasiewicz and Stoń-Egiert 2016) and
780 chlorophyll fluorescence to be low (Seppälä et al. 2007). Florida Bay *Synechococcus* blooms
781 exhibited high $a^*_{ph}(675)$ (~0.018 ± 0.001 m^2 mg^{-1}) attributed to strong pigment absorption and
782 weak pigment packaging and low chlorophyll-a fluorescence based on strong spectral agreement
783 between $R_{rs}(\lambda)$ and $1/a_{tot}(\lambda)$, helping to explain why CI_{MODIS} was positive for these blooms.
784 High scattering in freshwater *Microcystis* blooms leads to increased reflectance at near-
785 IR wavelengths (Moore et al. 2017), also helping to explain why CI is positive. Less is known
786 regarding the scattering properties of natural *Synechococcus* bloom populations owing to a lack
787 of measurements. However, studies performed on cultures revealed high chlorophyll-specific
788 particulate scattering coefficients attributed to their small cell size that leads to enhanced
789 reflectance at red and near-IR wavelengths (Soja-Woźniak et al. 2017; Wojtasiewicz and Stoń-
790 Egiert 2016). Further inferences on the scattering properties of natural *Synechococcus* blooms
791 can be made based on knowledge of cellular structure and certain physiological adaptations.

792 TEM micrographs of natural *Synechococcus* bloom populations in Florida Bay revealed the
793 presence of gas vacuoles for buoyancy control (Phlips et al. 1999) that are known to strongly
794 scatter light (Ganf et al. 1989). Also, natural bloom populations of *Synechococcus* produce and
795 excrete a sticky, carbohydrate polymer (Phlips et al. 1989), which has been linked to increased
796 scattering in other phytoplankton types (Tassan 1993). This material may serve as a defence
797 mechanism against predation and protect cells from being damaged by high light (Berry et al.
798 2015).

799 Unlike most inland and coastal systems for which cyanobacteria bloom detection
800 algorithms have previously been developed, shallow coastal lagoons often contain vast areas of
801 dense seagrass or macrophyte beds with low overlying water column attenuation, resulting in
802 strong bottom reflectance contributions. In Florida Bay, these areas also often exhibit positive
803 CI_{MODIS} because the strong red-edge reflectance of submerged aquatic vegetation can propagate
804 to the surface even after water-column attenuation in waters < 1-2 m deep (Bostater et al. 2004).
805 This problem was especially prevalent on mud bank margins in WFB where seagrass beds are
806 especially dense (Prager and Halley 1999) and may be exacerbated during the dry season
807 (December - May) when sea level in Florida Bay is lower by ~30cm (Lee et al. 2016).

808 The highly negative SS(488) exhibited by cyanobacteria blooms in Florida Bay was
809 shown to be unique compared to other optical water types, allowing for this feature to help
810 discriminate between weaker blooms with Chl_{CI} < 10 mg m^{-3} and shallow regions with dense
811 seagrass and high bottom reflectance contributions. Negative SS(488) in cyanobacteria blooms
812 was attributed to high carotenoid absorption, low pigment packaging, and low detrital
813 absorption. Because these blooms typically occur in calm (non-turbid) shallow waters with long
814 residence times that are exposed to high photic flux, cells manufacture high concentrations of

photoprotective carotenoids (PPC; zeaxanthin and β-carotene) that strongly absorb light at ~490nm. This helps to protect cellular machinery from the damaging effects of photo-oxidation. The paucity of CDOM in this region, which acts as a natural sunscreen, may explain why PPC/Chl-a was higher here than in nearby CDOM-rich, river-dominated estuaries (Louda 2007).

Negative SS(488) (or SS(490)) has also been observed in high-biomass red tide blooms dominated by *Karenia brevis* (Tomlinson et al. 2009). These blooms are often transported southward along the West Florida Shelf and into GFB during fall and winter, occasionally forming so-called "black water" events (Neely et al. 2004; Zhao et al. 2013). However, because red tides exhibit positive MODIS FLH (Hu et al. 2005), misclassification of red tides as cyanobacteria blooms using the modified CI approach is unlikely because CI_{MODIS} would be negative.

5.2 Strengths and weaknesses of the new approach

The modified CI approach has several strengths, including its ability to discriminate between different bloom types and perform accurately in optically shallow waters. Results presented above from model simulations and image-based analysis indicated that this approach will perform accurately for a wide range of aerosols and sensor viewing geometries. Perturbations caused by CDOM and resuspended sediments are also not expected to have large impacts on algorithm performance, as discussed below.

For perturbations by CDOM, model simulations by McKee et al. (2007) showed that a 20-fold increase in CDOM absorption only resulted in a 50% reduction in MODIS FLH (equivalent to negative CI_{MODIS}). Although CDOM variability will likely have a greater impact on SS(488) than on CI_{MODIS}, $a_{CDOM}(443)$ was relatively low (<0.8 m^{-1}) and varied minimally (~5-

838 fold) in Florida Bay compared to nearby river-dominated estuaries (Cannizzaro et al. 2013a; Le
839 et al. 2013). This indicated the likelihood of minimal impacts of CDOM on algorithm
840 performance. Measurements presented here were consistent with previous reports that showed
841 relatively low CDOM absorption and fluorescence originating mainly from marine sources
842 (seagrasses and phytoplankton) that covered a small dynamic range (Maie et al. 2006;
843 McPherson et al. 2011).

844 For perturbations by resuspended sediments such as after extreme storm events (e.g.,
845 winter cold fronts and summer/fall tropical storms) (Conmy et al. 2009), false positive
846 classification of post-storm turbid waters as cyanobacteria blooms using the new approach is
847 highly unlikely because high sediment loads will cause a false "fluorescence" signal, leading to
848 positive MODIS FLH (equivalent to negative CI_{MODIS}) (Gilerson et al. 2007). Also, high
849 concentrations of resuspended sediments will not cause the concave spectral curvature in
850 reflectance between 440 and 550 nm (Fig. 3), and so both the use of CI_{MODIS} and SS(488) would
851 rule out these waters as blooms.

852 The tolerance of the new approach to perturbations by post-storm sediment resuspension
853 is illustrated for south Florida coastal and estuarine waters in the example in Figure 14. In this
854 comparison between MODIS/Aqua RGB and Chl_{CI} imagery collected on 20 January 2017 (two
855 days prior to a winter storm event) and on 24 January 2017 (two days after a winter storm event),
856 significant sediment resuspension in the latter case did not significantly alter the bloom patterns
857 as shown in both the images and the histograms, although slight changes in bloom position and
858 strength might be a result of water movement both vertically and horizontally. High wind stress
859 also led to changes in the areal extent and magnitude of cyanobacteria blooms in the U.S. Great
860 Lakes caused by mixing of cells throughout the water column (Wynne et al. 2010).

The new approach does have several limitations, however. Perturbations in algorithm performance caused by high sun glint (L_g > 0.005 sr^{-1}, threshold used by NASA to indicate "high glint" in SeaDAS processing) are expected during summer for this subtropical location. Sun glint is known to cause problems for many remote sensing algorithms because it not only leads to increased $R_{rc}(\lambda)$ but also modifies the spectral shape. However, because of the linear baseline subtraction design in both CI_{MODIS} and SS(488), the approach appears to be tolerant to sun glint for L_g < 0.005 sr^{-1}. This is similar to the tolerance of the 443-555-670 band difference approach used to estimate open-ocean Chl-a (Hu et al. 2012b). For L_g > 0.01 sr^{-1}, the MODIS 678-nm band often saturates because of its high sensitivity and low saturation threshold (Hu et al. 2012a), leading to no retrievals.

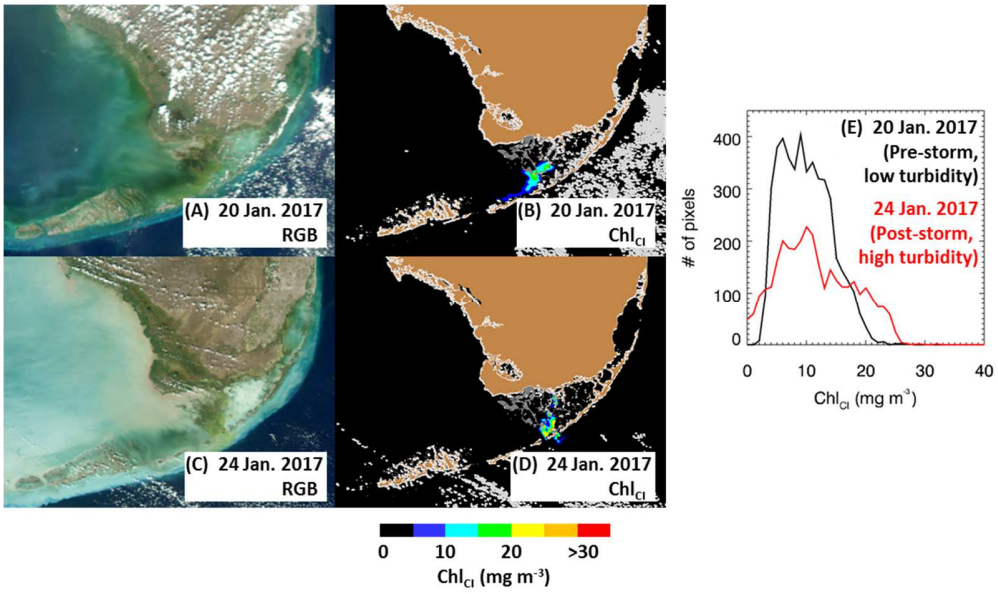

Figure 14. Example showing how the modified CI approach is affected by turbidity. (a) and (b) show MODIS/Aqua RGB-composite image and Chl_{CI} (mg m^{-3}) on 20 January 2017 (pre-storm with low turbidity). (c) and (d) show MODIS/Aqua RGB-composite image and Chl_{CI} (mg m^{-3}) on 24 January 2017 (post-storm with high turbidity). The histograms in (e) show Chl_{CI} distribution statistics on 20 January 2017 (black) and 24 January 2017 (red) for areas positively classified as cyanobacteria blooms.

879 Another limitation is that cyanobacterial blooms are known to exhibit extreme horizontal
880 patchiness (Kutser 2004). Consequently, the 1-km resolution MODIS bands may not be
881 sufficient to capture small bloom patches, making it difficult to detect bloom initiation. The 1-km
882 resolution of MODIS also makes it difficult to assess the spatial and temporal distributions of
883 cyanobacteria blooms that occur in the small (~1-10 km^2) saline lakes and embayments located
884 along the mainland shore of northern Florida Bay (Frankovich et al. 2017). These areas are of
885 special interest because they're considered to be particularly sensitive to flow increases that
886 began in 2012 as part of the C-111 Spreader Canal Western Features project (South Florida
887 Water Management District), one of the first phases of CERP (Shangguan et al. 2017).
888
889 ***5.3 Applicability to other regions***
890 Coastal lagoons rank among the most biologically productive marine systems and often
891 exhibit high ecologic, recreation, and commercial value. Picocyanobacteria are especially well-
892 adapted to changing environmental conditions found in these systems given their small size,
893 euryhaline character, buoyancy, and tolerance to high light intensity (Phlips et al. 1999). Global
894 expansion of cyanobacteria blooms has been linked to eutrophication and climate change, posing
895 major threats to ecosystems worldwide (O'Neil et al. 2012; Paerl and Huisman 2009).
896 Marine picocyanobacteria blooms dominated by *Synechococcus* have occurred in several
897 other coastal lagoons and estuaries, causing widespread disruption to ecosystems and negative
898 socioeconomic effects. These regions include the Gippsland Lakes (Australia) (Cook and
899 Holland 2012), Mar Menor (Spain) (Pérez-Ruzafa et al. 2019), Laguna Madre (U.S.A) (Buskey
900 et al. 2001), and Guantánamo Bay (Cuba) (Hall et al. 2018). Similarly, picocyanobacteria blooms
901 dominated by freshwater/brackish genera have been reported in river-dominated coastal lagoons

902 and estuaries, including Patos Lagoon (Brazil) (De Souza et al. 2018), Pensacola Bay (U.S.A),
903 Swan River Estuary (Australia) (Robson and Hamilton 2003), and Curonian Lagoon (Baltic Sea)
904 (Belykh et al. 2013). These latter blooms typically occur during the summer following the
905 demise of spring phytoplankton blooms, which are dominated by larger-sized phytoplankton
906 (i.e., >10 μm).
907 While algorithm tuning may be required for these other systems because each region may
908 exhibit its own unique optical complexity, the general approach to combine CI_{MODIS} and SS(488)
909 is expected to work, especially in CDOM-poor regions exposed to high photic flux where
910 PPC/Chl-a is high, causing SS(488) to be low. Otherwise, the original CI approach may be
911 sufficient for detecting blooms in highly-attenuating, CDOM-rich regions with minimal bottom
912 reflectance contributions.
913
914 ***5.4 Future work***
915 In addition to using MODIS for detecting and quantifying cyanobacteria blooms in
916 Florida Bay, it is desirable to use other sensors, especially those with higher spectral or spatial
917 resolutions, to develop band-specific or sensor-specific methods. Alternative sensors may
918 include ENVISAT MERIS, Sentinel-3 OLCI, Landsat sensors, and Sentinel-2 MSI. While
919 MERIS and OLCI are equipped with more spectral bands than MODIS and include the 620-nm
920 band that is sensitive to PC, Landsat sensors and MSI have much higher spatial resolutions (30-
921 m and 10-m, respectively) for detecting small bloom patches, but at the price of lower spectral
922 resolution and less-frequent coverage. The use of Landsat series can also track historical bloom
923 events back to the 1980's. Altogether, these various satellite sensors may provide a seamless
924 long-term data record of cyanobacterial blooms after further algorithm development (e.g., Sun et

al. 2015; Vincent et al. 2004) and cross-sensor calibration (e.g., Ho et al. 2017), making it possible to study these blooms when they first appeared in the 1990's (Boyer et al. 1999; Phlips et al. 1999).

Once a long-term data record is established, the hypothesis that reductions to natural sheet flow from ENP into Florida Bay is the main causative factor leading up to blooms can be tested with other environmental data. Similarly, monitoring blooms with improved spatial and temporal coverage, as enabled by this established approach, is critical toward determining the response of phytoplankton populations to increased freshwater flow as part of federal/state restoration efforts (Butler and Dolan 2017; Shangguan et al. 2017). Information on the spatial and temporal distribution of blooms can also be embedded into models for assessing the impacts of increased flow on lobster and sponge populations (Butler and Dolan 2017). Currently, such models do not include cyanobacteria blooms in GFB because of a lack of field measurements in this region, yet results presented in Figures 9 and 13 indicate that cyanobacteria blooms may extend westward into S-GFB in fall and winter. Local management agencies may also use this information for identifying suitable restoration sites for sponge and coral nurseries where historical bloom activity is minimal and for modelling the submarine light environment for seagrasses community assessments. Overall, the approach developed here is expected to lead to improved monitoring and management strategies, allowing management agencies to better serve and protect natural resources.

6. Conclusions

Based on analyses of bio-optical properties of Florida Bay waters, reflectance spectra of various optical water types, including picocyanobacteria blooms dominated by *Synechococcus*,

948 are characterized. Unique spectral shapes are found for these blooms, which lead to the
949 development of a new cyanobacteria bloom detection and quantification method through the use
950 of two spectral shape indexes, one focused on red-NIR bands (CI_{MODIS} (Wynne et al. 2013)) and
951 the other on blue-green bands (SS(488)). Compared to the original CI approach, the method
952 shows improved performance, with 75% of cyanobacteria blooms successfully classified for
953 Chl_{CI} ranging between ~5 and 40 mg m^{-3}. The success of the new modified CI approach suggests
954 that its application to the long-term MODIS time-series may lead to the establishment of a
955 unique dataset for studying the causes of historical blooms in Florida Bay and monitoring
956 potential impacts of future increased flow from upstream waters in ENP associated with the
957 current federal restoration effort. Furthermore, it may be a potentially robust method for
958 detecting picocyanobacteria blooms in other optically complex lagoons and estuaries prone to
959 high bottom reflectance contributions where these blooms are known to occur.
960

961 **Acknowledgments**

962 This work was supported by the U.S. NASA Ocean Biology and Biogeochemistry
963 program (NNX14AL98G, NNX16AR74G) and Ecological Forecast program (NNX17AE57G)
964 and by the U.S. NOAA STAR (NA15OAR4320064). We thank NASA GSFC for providing
965 MODIS data used in the analysis here and NOAA/COP for providing support for the 1997-1998
966 field work. Support for field data collected as part of NOAA-AOML's SFP was provided by the
967 NOAA/OAR Ship Charter Fund, NOAA's Center for Sponsored Coastal Ocean Research,
968 NOAA's Deepwater Horizon Supplemental Appropriation, and the U.S. Army Corps of
969 Engineers. Two anonymous reviewers provided extensive comments and suggestions to improve
970 the presentation of this work, whose effort is greatly appreciated.

971 **References**

972 Barnes, B.B., Hu, C., Holekamp, K.L., Blonski, S., Spiering, B.A., Palandro, D., & Lapointe, B.
973 (2014). Use of Landsat data to track historical water quality changes in Florida Keys marine
974 environments. *Remote Sensing of Environment, 140*, 485-496

975 Belykh, O., Dmitrieva, O., Gladkikh, A., & Sorokovikova, E. (2013). Identification of toxigenic
976 cyanobacteria of the genus *Microcystis* in the Curonian Lagoon (Baltic Sea). *Oceanology, 53*,
977 71-79

978 Berry, D.L., Goleski, J.A., Koch, F., Wall, C.C., Peterson, B.J., Anderson, O.R., & Gobler, C.J.
979 (2015). Shifts in cyanobacterial strain dominance during the onset of harmful algal blooms in
980 Florida Bay, USA. *Microbial ecology, 70*, 361-371

981 Blakey, T., Melesse, A., Sukop, M.C., Tachiev, G., Whitman, D., & Miralles-Wilhelm, F.
982 (2016). Developing benthic class specific, chlorophyll-a retrieving algorithms for optically-
983 shallow water using SeaWiFS. *Sensors, 16*, 1749

984 Blondeau-Patissier, D., Gower, J.F., Dekker, A.G., Phinn, S.R., & Brando, V.E. (2014). A
985 review of ocean color remote sensing methods and statistical techniques for the detection,
986 mapping and analysis of phytoplankton blooms in coastal and open oceans. *Progress in*
987 *Oceanography, 123*, 123-144

988 Bostater, C.R., Ghir, T., Bassetti, L., Hall, C., Reyeier, E., Lowers, R., Holloway-Adkins, K., &
989 Virnstein, R. (2004). Hyperspectral remote sensing protocol development for submerged
990 aquatic vegetation in shallow waters. In, *Remote Sensing of the Ocean and Sea Ice 2003,*
991 *Proc. SPIE 5233* (pp. 199-215)

992 Boyer, J.N., Fourqurean, J.W., & Jones, R.D. (1997). Spatial characterization of water quality in
993 Florida Bay and Whitewater Bay by multivariate analyses: zones of similar influence.
994 *Estuaries, 20*, 743-758
995 Boyer, J.N., Fourqurean, J.W., & Jones, R.D. (1999). Seasonal and long-term trends in the water
996 quality of Florida Bay (1989–1997). *Estuaries, 22*, 417-430
997 Boyer, J.N., Kelble, C.R., Ortner, P.B., & Rudnick, D.T. (2009). Phytoplankton bloom status:
998 Chlorophyll a biomass as an indicator of water quality condition in the southern estuaries of
999 Florida, USA. *Ecological Indicators, 9*, S56-S67
1000 Brand, L.E. (2002). The transport of terrestrial nutrients to South Florida coastal waters. In J.W.
1001 Porter, & K.G. Porter (Eds.), *The Everglades, Florida Bay, and Coral Reefs of the Florida*
1002 *Keys: An Ecosystem Sourcebook* (pp. 361-413). Boca Raton, FL: CRC Press
1003 Brand, L.E., Pablo, J., Compton, A., Hammerschlag, N., & Mash, D.C. (2010). Cyanobacterial
1004 blooms and the occurrence of the neurotoxin, beta-N-methylamino-l-alanine (BMAA), in
1005 South Florida aquatic food webs. *Harmful Algae, 9*, 620-635
1006 Bricaud, A., Claustre, H., Ras, J., & Oubelkheir, K. (2004). Natural variability of
1007 phytoplanktonic absorption in oceanic waters: Influence of the size structure of algal
1008 populations. *Journal of Geophysical Research: Oceans, 109*, doi:10.1029/2004JC002419
1009 Briceño, H.O., & Boyer, J.N. (2009). Climatic controls on phytoplankton biomass in a sub-
1010 tropical estuary, Florida Bay, USA. *Estuaries and Coasts, 33*, 541-553
1011 Buskey, E.J., Liu, H., Collumb, C., & Bersano, J.G.F. (2001). The decline and recovery of a
1012 persistent Texas brown tide algal bloom in the Laguna Madre (Texas, USA). *Estuaries, 24*,
1013 337-346

1014 Butler, M.J., & Dolan, T.W. (2017). Potential Impacts of Everglades Restoration on Lobster and
1015 Hard Bottom Communities in the Florida Keys, FL (USA). *Estuaries and Coasts, 40*, 1523-
1016 1539
1017 Butler, M.J., Hunt, J.H., Herrnkind, W.F., Childress, M.J., Bertelsen, R., Sharp, W., Matthews,
1018 T., Field, J.M., & Marshall, H.G. (1995). Cascading disturbances in Florida Bay, USA:
1019 cyanobacteria blooms, sponge mortality, and implications for juvenile spiny lobsters
1020 *Panulirus argus*. *Marine Ecology Progress Series, 129*, 119-125
1021 Cannizzaro, J.P., Carlson Jr, P.R., Yarbro, L.A., & Hu, C. (2013a). Optical variability along a
1022 river plume gradient: Implications for management and remote sensing. *Estuarine, Coastal*
1023 *and Shelf Science, 131*, 149-161
1024 Cannizzaro, J.P., Hu, C., Carder, K.L., Kelble, C.R., Melo, N., Johns, E.M., Vargo, G.A., & Heil,
1025 C.A. (2013b). On the accuracy of SeaWiFS ocean color data products on the West Florida
1026 Shelf. *Journal of Coastal Research, 29*, 1257-1272
1027 Carder, K.L., Hawes, S.K., Baker, K.A., Smith, R.C., Steward, R.G., & Mitchell, B.G. (1991).
1028 Reflectance model for quantifying chlorophyll a in the presence of productivity degradation
1029 products. *Journal of Geophysical Research: Oceans, 96*, 20599-20611
1030 Conmy, R.N., Coble, P.G., Cannizzaro, J.P., & Heil, C.A. (2009). Influence of extreme storm
1031 events on West Florida Shelf CDOM distributions. *Journal of Geophysical Research, 114*,
1032 doi:10.1029/2009JG000981
1033 Cook, P.L., & Holland, D.P. (2012). Long term nutrient loads and chlorophyll dynamics in a
1034 large temperate Australian lagoon system affected by recurring blooms of cyanobacteria.
1035 *Biogeochemistry, 107*, 261-274

1036 Cullen, J.J., Ciotti, A.M., Davis, R.F., & Lewis, M.R. (1997). Optical detection and assessment
1037 of algal blooms. *Limnology and Oceanography, 42*, 1223-1239
1038 D'Sa, E.J., Hu, C., Müller-Karger, F.E., & Carder, K.L. (2002). Estimation of colored dissolved
1039 organic matter and salinity fields in case 2 waters using SeaWiFS: Examples from Florida
1040 Bay and Florida Shelf. *Journal of Earth System Science, 111*, 197-207
1041 De Souza, M.S., Muelbert, J.H., Costa, L.D.F., Klering, E.V., & Yunes, J.S. (2018).
1042 Environmental variability and cyanobacterial blooms in a subtropical coastal lagoon:
1043 searching for a sign of climate change effects. *Frontiers in Microbiology, 9*, 1-12
1044 Dekker, A.G. (1993). Detection of optical water quality parameters for eutrophic waters by high
1045 resolution remote sensing. In (p. 222). Amsterdam: Vrije Universiteit
1046 Evans, S.L., Anderson, W.T., & Jochem, F.J. (2006). Spatial variability in Florida Bay
1047 particulate organic matter composition: combining flow cytometry with stable isotope
1048 analyses. *Hydrobiologia, 569*, 151-165
1049 Feng, L., & Hu, C. (2017). Land adjacency effects on MODIS Aqua top-of-atmosphere radiance
1050 in the shortwave infrared: Statistical assessment and correction. *Journal of Geophysical*
1051 *Research: Oceans, 122*, 4802-4818
1052 Fourqurean, J.W., & Robblee, M.B. (1999). Florida Bay: a history of recent ecological changes.
1053 *Estuaries and Coasts, 22*, 345-357
1054 Frankovich, T.A., Rudnick, D.T., & Fourqurean, J.W. (2017). Light attenuation in estuarine
1055 mangrove lakes. *Estuarine, Coastal and Shelf Science, 184*, 191-201
1056 Ganf, G., Oliver, R., & Walsby, A. (1989). Optical properties of gas-vacuolate cells and colonies
1057 of *Microcystis* in relation to light attenuation in a turbid, stratified reservoir (Mount Bold
1058 Reservoir, South Australia). *Marine and Freshwater Research, 40*, 595-611

1059 Gao, B.-C., Montes, M.J., Li, R.-R., Dierssen, H.M., & Davis, C.O. (2007). An atmospheric
1060 correction algorithm for remote sensing of bright coastal waters using MODIS land and
1061 ocean channels in the solar spectral region. *IEEE Transactions on Geoscience and Remote*
1062 *Sensing, 45*, 1835-1843
1063 Gardner, W.S., & McCarthy, M.J. (2009). Nitrogen dynamics at the sediment–water interface in
1064 shallow, sub-tropical Florida Bay: why denitrification efficiency may decrease with
1065 increased eutrophication. *Biogeochemistry, 95*, 185-198
1066 Gérikas Ribeiro, C., Marie, D., Lopes dos Santos, A., Pereira Brandini, F., & Vaulot, D. (2016).
1067 Estimating microbial populations by flow cytometry: Comparison between instruments.
1068 *Limnology and Oceanography: Methods, 14*, 750-758
1069 Gilerson, A., Zhou, J., Hlaing, S., Ioannou, I., Schalles, J., Gross, B., Moshary, F., & Ahmed, S.
1070 (2007). Fluorescence component in the reflectance spectra from coastal waters. Dependence
1071 on water composition. *Optics Express, 15*, 15702-17721
1072 Glibert, P., Heil, C.A., Hollander, D., Revilla, M., Hoare, A., Alexander, J., & Murasko, S.
1073 (2004). Evidence for dissolved organic nitrogen and phosphorus uptake during a
1074 cyanobacterial bloom in Florida Bay. *Marine Ecology Progress Series, 280*, 73-83
1075 Glibert, P.M., Heil, C.A., Rudnick, D., Madden, C.J., Boyer, J.N., & Kelly, S. (2009). Florida
1076 Bay: water quality status and trends, historic and emerging algal bloom problems.
1077 *Contributions in Marine Science, 38*, 5-17
1078 Goleski, J.A., Koch, F., Marcoval, M.A., Wall, C.C., Jochem, F.J., Peterson, B.J., & Gobler, C.J.
1079 (2010). The role of zooplankton grazing and nutrient loading in the occurrence of harmful
1080 cyanobacterial blooms in Florida Bay, USA. *Estuaries and Coasts, 35*, 1202-1215

1081 Gower, J.F., Brown, L., & Borstad, G.A. (2004). Observation of chlorophyll fluorescence in west
1082 coast waters of Canada using the MODIS satellite sensor. *Canadian Journal of Remote*
1083 *Sensing, 30*, 17-25
1084 Hall, M.O., Durako, M.J., Fourqurean, J.W., & J.C.Zieman (1999). Decadal changes in seagrass
1085 distribution and abundance in Florida Bay. *Estuaries, 22*, 445-459
1086 Hall, M.O., Furman, B.T., Merello, M., & Durako, M.J. (2016). Recurrence of *Thalassia*
1087 *testudinum* seagrass die-off in Florida Bay, USA: Initial observations. *Marine Ecology*
1088 *Progress Series, 560*, 243-249
1089 Hall, N.S., Litaker, R.W., Kenworthy, W.J., Vandersea, M.W., Sunda, W.G., Reid, J.P., Slone,
1090 D.H., & Butler, S. (2018). Consortial brown tide– picocyanobacteria blooms in Guantánamo
1091 Bay, Cuba. *Harmful Algae, 73*, 30-43
1092 Hitchcock, G., Phlips, E., Brand, L., & Morrison, D. (2007). Plankton blooms. In J. Hunt, & W.
1093 Nuttle (Eds.), *Florida Bay Science Program: A Synthesis of Research on Florida Bay* (pp.
1094 77-91). St. Petersburg, FL: Florida Fish and Wildlife Conservation Commission, Fish and
1095 Wildlife Research Institute
1096 Ho, J.C., Stumpf, R.P., Bridgeman, T.B., & Michalak, A.M. (2017). Using Landsat to extend the
1097 historical record of lacustrine phytoplankton blooms: A Lake Erie case study. *Remote*
1098 *Sensing of Environment, 191*, 273-285
1099 Hoepffner, N., & Sathyendranath, S. (1991). Effect of pigment composition on absorption
1100 properties of phytoplankton. *Marine Ecology Progress Series, 73*, 11-23
1101 Holm-Hansen, O., & Riemann, B. (1978). Chlorophyll a determination: improvements in
1102 methodology. *Oikos, 30*, 438-447

1103 Hu, C. (2009). A novel ocean color index to detect floating algae in the global oceans. *Remote*
1104 *Sensing Environment, 113*, 2118-2129
1105 Hu, C. (2011). An empirical approach to derive MODIS ocean color patterns under severe sun
1106 glint. *Geophysical Research Letters, 38*, L01603
1107 Hu, C., Feng, L., Lee, Z., Davis, C.O., Mannino, A., McClain, C.R., & Franz, B.A. (2012a).
1108 Dynamic range and sensitivity requirements of satellite ocean color sensors: Learning from
1109 the past. *Applied Optics, 51*, 6045-6062
1110 Hu, C., Lee, Z., & Franz, B. (2012b). Chlorophyll algorithms for oligotrophic oceans: A novel
1111 approach based on three-band reflectance difference. *Journal of Geophysical Research:*
1112 *Oceans, 117*, doi:10.1029/2011JC007395
1113 Hu, C., Müller-Karger, F.E., Taylor, C., Carder, K.L., Kelble, C., Johns, E., & Heil, C.A. (2005).
1114 Red tide detection and tracing using MODIS fluorescence data: An example in SW Florida
1115 coastal waters. *Remote Sensing of Environment, 97*, 311-321
1116 Hunter, P.D., Tyler, A.N., Gilvear, D.J., & Willby, N.J. (2009). Using remote sensing to aid the
1117 assessment of human health risks from blooms of potentially toxic cyanobacteria.
1118 *Environmental Science & Technology, 43*, 2627-2633
1119 Johnsen, G., & Sakshaug, E. (1996). Light harvesting in bloom-forming marine phytoplankton:
1120 species-specificity and photoacclimation. *Scientia Marina, 60*, 47-56
1121 Jurado, J.L., Hitchcock, G.L., & Ortner, P.B. (2007). Seasonal variability in nutrient and
1122 phytoplankton distribution on the southwest Florida inner shelf. *Bulletin of Marine Science,*
1123 *80*, 21-43
1124 Kelble, C.R., Johns, E.M., Nuttle, W.K., Lee, T.N., Smith, R.H., & Ortner, P.B. (2007). Salinity
1125 patterns of Florida Bay. *Estuarine, Coastal and Shelf Science, 71*, 318-334

1126 Kelble, C.R., Ortner, P.B., Hitchcock, G.L., & Boyer, J.N. (2005). Attenuation of
1127 photosynthetically available radiation (PAR) in Florida Bay: Potential for light limitation of
1128 primary producers. *Estuaries, 28*, 560-571
1129 Kiefer, D.A., & SooHoo, J.B. (1982). Spectral absorption by marine particles of coastal waters of
1130 Baja California. *Limnology and Oceanography, 27*, 492-499
1131 Kirk, J.T.O. (1994). *Light and Photosynthesis in Aquatic Ecosystems*. Cambridge: Cambridge
1132 University Press
1133 Kishino, M., Takahashi, M., Okami, N., & Ichimura, S. (1985). Estimation of the spectral
1134 absorption coefficients of phytoplankton in the sea. *Bulletin of Marine Science, 37*, 634-642
1135 Kohavi, R., & Provost, F. (1998). Glossary of Terms. *Machine Learning, 30*, 271-274
1136 Kutser, T. (2004). Quantitative detection of chlorophyll in cyanobacterial blooms by satellite
1137 remote sensing. *Limnology and Oceanography, 49*, 2179-2189
1138 Kutser, T., Metsamaa, L., Strömbeck, N., & Vahtmäe, E. (2006). Monitoring cyanobacterial
1139 blooms by satellite remote sensing. *Estuarine, Coastal and Shelf Science, 67*, 303-312
1140 Le, C., Hu, C., English, D., Cannizzaro, J., Chen, Z., Kovach, C., Anastasiou, C.J., Zhao, J., &
1141 Carder, K.L. (2013). Inherent and apparent optical properties of the complex estuarine waters
1142 of Tampa Bay: What controls light? *Estuarine, Coastal and Shelf Science, 117*, 54-69
1143 Lee, T.N., Johns, E., Melo, N., Smith, R.H., Ortner, P., & Smith, D. (2006). On Florida Bay
1144 hypersalinity and water exchange. *Bulletin of Marine Science, 79*, 301-327
1145 Lee, T.N., Melo, N., Johns, E., Kelble, C., Smith, R.H., & Ortner, P. (2008). On water renewal
1146 and salinity variability in the northeast subregion of Florida Bay. *Bulletin of Marine Science,*
1147 *82*, 83-105

1148 Lee, T.N., Melo, N., Smith, N., Johns, E.M., Kelble, C.R., Smith, R.H., & Ortner, P.B. (2016).
1149 Circulation and water renewal of Florida Bay, USA. *Bulletin of Marine Science, 92*, 153-180
1150 Lee, Z., Ahn, Y., Mobley, C., & Arnone, R. (2010). Removal of surface-reflected light for the
1151 measurement of remote-sensing reflectance from an above-surface platform. *Optics Express,*
1152 *18*, 26313-26324
1153 Lee, Z., Carder, K.L., Chen, R.F., & Peacock, T.G. (2001). Properties of the water column and
1154 bottom derived from Airborne Visible Infrared Imaging Spectrometer (AVIRIS) data.
1155 *Journal of Geophysical Research: Oceans, 106*, 11639-11651
1156 Letelier, R.M., & Abbott, M.R. (1996). An analysis of chlorophyll fluorescence algorithms for
1157 the Moderate Resolution Imaging Spectrometer (MODIS). *Remote Sensing of Environment,*
1158 *58*, 215-223
1159 Light, S.S., & Dineen, J.W. (1994). Water control in the Everglades: A historical perspective. In
1160 S.M. Davis, & J.C. Ogden (Eds.), *Everglades: The ecosystem and its restoration* (pp. 47-84).
1161 Boca Raton, FL: St. Lucie Press
1162 Louda, J.W. (2007). HPLC-based chemotaxonomy of Florida Bay phytoplankton: Difficulties in
1163 coastal environments. *Journal of Liquid Chromatography & Related Technologies, 31*, 295-
1164 323
1165 Lunetta, R.S., Schaeffer, B.A., Stumpf, R.P., Keith, D., Jacobs, S.A., & Murphy, M.S. (2015).
1166 Evaluation of cyanobacteria cell count detection derived from MERIS imagery across the
1167 eastern USA. *Remote Sensing of Environment, 157*, 24-34
1168 Maie, N., Boyer, J.N., Yang, C., & Jaffe, R. (2006). Spatial, geomorphological, and seasonal
1169 variability of CDOM in estuaries of the Florida Coastal Everglades. *Hydrobiologia, 569*,
1170 135-150

1171 Marie, D., Partensky, F., Jacquet, S., & Vaulot, D. (1997). Enumeration and cell cycle analysis
1172 of natural populations of marine picoplankton by flow cytometry using the nucleic acid stain
1173 SYBR Green I. *Applied and Environmental Microbiology, 63*, 186-193
1174 Marie, D., Simon, N., & Vaulot, D. (2005). Phytoplankton cell counting by flow cytometry. In
1175 R.A. Andersen (Ed.), *Algal culturing techniques* (pp. 253-267). Amsterdam: Elsevier
1176 Matthews, M.W., Bernard, S., & Robertson, L. (2012). An algorithm for detecting trophic status
1177 (chlorophyll-*a*), cyanobacterial-dominance, surface scums and floating vegetation in inland
1178 and coastal waters. *Remote Sensing of Environment, 124*, 637-652
1179 Matthews, M.W., & Odermatt, D. (2015). Improved algorithm for routine monitoring of
1180 cyanobacteria and eutrophication in inland and near-coastal waters. *Remote Sensing of*
1181 *Environment, 156*, 374-382
1182 McKee, D., Cunningham, A., Wright, D., & Hay, L. (2007). Potential impacts of nonalgal
1183 materials on water-leaving Sun induced chlorophyll fluorescence signals in coastal waters.
1184 *Applied Optics, 46*, 7720-7729
1185 McPherson, M.L., Hill, V.J., Zimmerman, R.C., & Dierssen, H.M. (2011). The optical properties
1186 of Greater Florida Bay: Implications for seagrass abundance. *Estuaries and Coasts, 34*, 1150-
1187 1160
1188 Millette, N., Kelble, C., Linhoss, A., Ashby, S., & Visser, L. (2018). Shift in baseline chlorophyll
1189 a concentration following a three-year *Synechococcus* bloom in southeastern Florida. *Bulletin*
1190 *of Marine Science, 94*, 3-19
1191 Moore, T.S., Mouw, C.B., Sullivan, J.M., Twardowski, M.S., Burtner, A.M., Ciochetto, A.B.,
1192 McFarland, M.N., Nayak, A.R., Paladino, D., Stockley, N.D., & Johengen, T.H. (2017). Bio-

optical properties of cyanobacteria blooms in Western Lake Erie. *Frontiers in Marine Science, 4:300. doi: 10.3389/fmars.2017.00300*

Moradi, M. (2014). Comparison of the efficacy of MODIS and MERIS data for detecting cyanobacterial blooms in the southern Caspian Sea. *Marine Pollution Bulletin, 87*, 311-322

Morel, A., & Bricaud, A. (1981). Theoretical results concerning light absorption in a discrete medium, and application to specific absorption of phytoplankton. *Deep Sea Research, 28*, 1375-1393

Morel, A., & Prieur, L. (1977). Analysis of variations in ocean color. *Limnology and Oceanography, 22*, 709-722

Mouw, C.B., Greb, S., Aurin, D., DiGiacomo, P.M., Lee, Z., Twardowski, M., Binding, C., Hu, C., Ma, R., & Moore, T. (2015). Aquatic color radiometry remote sensing of coastal and inland waters: Challenges and recommendations for future satellite missions. *Remote Sensing of Environment, 160*, 15-30

Neely, M.B., Bartels, E., Cannizzaro, J., Carder, K.L., Coble, P., English, D., Heil, C., Hu, C., Hunt, J., Ivey, J., McRae, G., Mueller, E., Peebles, E., & Steidinger, K. (2004). Florida's black water event. In J.H.L. K.A. Steidinger, C.R. Tomas, G.A. Vargo (Ed.), *Harmful Algae 2002* (pp. 377-379). St. Petersburg, FL, USA: Florida Fish and Wildlife Conservation Commission and Intergovernmental Oceanographic Commission of UNESCO

Nelson, N.G., Munoz-Carpena, R., & Phlips, E.J. (2017). A novel quantile method reveals spatiotemporal shifts in phytoplankton biomass descriptors between bloom and non-bloom conditions in a subtropical estuary. *Marine Ecology Progress Series, 567*, 57-78

1214 Nuttle, W.K., Fourqurean, J.W., Cosby, B.J., Zieman, J.C., & Robblee, M.B. (2000). Influence
1215 of net freshwater supply on salinity in Florida Bay. *Water Resources Research, 36*, 1805-
1216 1822
1217 O'Neil, J.M., Davis, T.W., Burford, M.A., & Gobler, C.J. (2012). The rise of harmful
1218 cyanobacteria blooms: the potential roles of eutrophication and climate change. *Harmful*
1219 *Algae, 14*, 313-334
1220 Paerl, H.W., & Huisman, J. (2009). Climate change: a catalyst for global expansion of harmful
1221 cyanobacterial blooms. *Environmental microbiology reports, 1*, 27-37
1222 Pérez-Ruzafa, A., Campillo, S., Fernández-Palacios, J.M., García Lacunza, A., García-Oliva, M.,
1223 Ibañez, H., Pérez-Marcos, M., Pérez-Ruzafa, I., Quispe, J.I., & Sala, A. (2019). Long term
1224 dynamic in nutrients, chlorophyll a and water quality parameters in a coastal lagoon during a
1225 process of eutrophication for decades, a sudden break and a relatively rapid recovery.
1226 *Frontiers in Marine Science, 6:26. doi: 10.3389/fmars.2019.00026*
1227 Phlips, E., Lynch, T., & Badylak, S. (1995). Chlorophyll a, tripton, color, and light availability in
1228 a shallow tropical inner-shelf lagoon, Florida Bay, USA. *Marine Ecology Progress Series,*
1229 *127*, 223-234
1230 Phlips, E.J., & Badylak, S. (1996). Spatial variability in phytoplankton standing crop and
1231 composition in a shallow inner-shelf lagoon, Florida Bay, Florida. *Bulletin of Marine*
1232 *Science, 58*, 203-216
1233 Phlips, E.J., Badylak, S., & Lynch, T.C. (1999). Blooms of the picoplanktonic cyanobacterium
1234 *Synechococcus* in Florida Bay, a subtropical inner-shelf lagoon. *Limnology and*
1235 *Oceanography, 44*, 1166-1175

1236 Phlips, E.J., Zeman, C., & Hansen, P. (1989). Growth, photosynthesis, nitrogen fixation and
1237 carbohydrate production by a unicellular cyanobacterium, *Synechococcus sp*. (Cyanophyta).
1238 *Journal of Applied Phycology, 1*, 137-145
1239 Pope, R., & Fry, E. (1997). Absorption spectrum (380-700nm) of pure waters: II. Integrating
1240 cavity measurements. *Applied Optics, 36*, 8710-8723
1241 Prager, E., & Halley, R.B. (1997). Florida Bay bottom types. In U.S.G. Survey (Ed.)
1242 Prager, E.J., & Halley, R.B. (1999). The Influence of Seagrass on Shell Layers and Florida Bay
1243 Mudbanks. *Journal of Coastal Research, 15*, 1151-1162
1244 Qi, L., Hu, C., Duan, H., Cannizzaro, J., & Ma, R. (2014). A novel MERIS algorithm to derive
1245 cyanobacterial phycocyanin pigment concentrations in a eutrophic lake: Theoretical basis and
1246 practical considerations. *Remote Sensing Environment, 154*, 298-317
1247 Rantajärvi, E., Olsonen, R., Hällfors, S., Leppänen, J.-M., & Raateoja, M. (1998). Effect of
1248 sampling frequency on detection of natural variability in phytoplankton: unattended high-
1249 frequency measurements on board ferries in the Baltic Sea. *ICES Journal of Marine Science,*
1250 *55*, 697-704
1251 Richardson, B. (2009). Physiological characteristics and competitive strategies of bloom-forming
1252 cyanobacteria and diatoms in Florida Bay. *Contrib. in Mar. Sci, 38*, 19-36
1253 Robson, B.J., & Hamilton, D.P. (2003). Summer flow event induces a cyanobacterial bloom in a
1254 seasonal Western Australian estuary. *Marine and Freshwater Research, 54*, 139-151
1255 Rudnick, D., Chen, Z., Childers, D., & Fontaine, T. (1999). Phosphorus and nitrogen inputs to
1256 Florida Bay: the importance of the Everglades watershed. *Estuaries, 22*, 398-416
1257 Rudnick, D.T., Ortner, P.B., Browder, J.A., & Davis, S.M. (2005). A conceptual ecological
1258 model of Florida Bay. *Wetlands, 25*, 870-883

1259 Schalles, J.F., & Yacobi, Y.Z. (2000). Remote detection and seasonal patterns of phycocyanin,
1260 carotenoid and chlorophyll pigments in eutrophic waters. *Ergebnisse Der Limnologie, 55*,
1261 153-168
1262 Seppälä, J., Ylöstalo, P., Kaitala, S., Hällfors, S., Raateoja, M., & Maunula, P. (2007). Ship-of-
1263 opportunity based phycocyanin fluorescence monitoring of the filamentous cyanobacteria
1264 bloom dynamics in the Baltic Sea. *Estuarine, Coastal and Shelf Science, 73*, 489-500
1265 Shangguan, Y., Glibert, P.M., Alexander, J.A., Madden, C.J., & Murasko, S. (2017). Nutrients
1266 and phytoplankton in semienclosed lagoon systems in Florida Bay and their responses to
1267 changes in flow from Everglades restoration. *Limnology and Oceanography, 62*, S327-S347
1268 Shoaf, W.T., & Lium, B.W. (1976). Improved extraction of chlorophyll a and b from algae using
1269 dimethyl sulfoxide. *Limnology and Oceanography, 21*, 926-928
1270 Simis, S.G., Peters, S.W., & Gons, H.J. (2005). Remote sensing of the cyanobacterial pigment
1271 phycocyanin in turbid inland water. *Limnology and Oceanography, 50*, 237-245
1272 Smith, N.P. (1997). An introduction to the tides of Florida Bay. *Florida Scientist, 60*, 53-67
1273 Soja-Woźniak, M., Darecki, M., Wojtasiewicz, B., & Bradtke, K. (2017). Laboratory
1274 measurements of remote sensing reflectance of selected phytoplankton species from the
1275 Baltic Sea. *Oceanologia, 60*, 86-96
1276 Stumpf, R.P., Frayer, M.L., Durako, M.J., & Brock, J.C. (1999). Variations in water clarity and
1277 bottom albedo in Florida Bay from 1985 to 1997. *Estuaries, 22*, 431-444
1278 Sun, D., Hu, C., Qiu, Z., & Shi, K. (2015). Estimating phycocyanin pigment concentration in
1279 productive inland waters using Landsat measurements: A case study in Lake Dianchi. *Optics*
1280 *Express, 23*, 3055-3074

1281 Tassan, S. (1993). An algorithm for the detection of the White-Tide ("mucilage") phenomenon in
1282 the Adriatic Sea using AVHRR data. *Remote Sensing of Environment, 45*, 29-42
1283 Tomlinson, M.C., Stumpf, R.P., Wynne, T.T., Dupuy, D., Burks, R., Hendrickson, J., & Fulton
1284 III, R.S. (2016). Relating chlorophyll from cyanobacteria-dominated inland waters to a
1285 MERIS bloom index. *Remote Sensing Letters, 7*, 141-149
1286 Tomlinson, M.C., Wynne, T.T., & Stumpf, R.P. (2009). An evaluation of remote sensing
1287 techniques for enhanced detection of the toxic dinoflagellate, *Karenia brevis*. *Remote*
1288 *Sensing of Environment, 113*, 598-609
1289 Vincent, R.K., Qin, X., McKay, R.M.L., Miner, J., Czajkowski, K., Savino, J., & Bridgeman, T.
1290 (2004). Phycocyanin detection from LANDSAT TM data for mapping cyanobacterial blooms
1291 in Lake Erie. *Remote Sensing of Environment, 89*, 381-392
1292 Wall, C.C., Rodgers, B.S., Gobler, C.J., & Peterson, B.J. (2012). Responses of loggerhead
1293 sponges *Spechiospongia vesparium* during harmful cyanobacterial blooms in a sub-tropical
1294 lagoon. *Marine Ecology Progress Series, 451*, 31-43
1295 Waterbury, J.B., Watson, S.W., Guillard, R.R., & Brand, L.E. (1979). Widespread occurrence of
1296 a unicellular, marine, planktonic, cyanobacterium. *Nature, 277*, 293-294
1297 Wojtasiewicz, B., & Stoń-Egiert, J. (2016). Bio-optical characterization of selected
1298 cyanobacteria strains present in marine and freshwater ecosystems. *Journal of Applied*
1299 *Phycology, 28*, 2299-2314
1300 Wozniak, S.B., & Stramski, D. (2004). Modeling the optical properties of mineral particles
1301 suspended in seawater and their influence on ocean reflectance and chlorophyll estimation
1302 from remote sensing algorithms. *Applied Optics, 43*, 3489-3503

Wynne, T.T., Stumpf, R.P., & Briggs, T.O. (2013). Comparing MODIS and MERIS spectral shapes for cyanobacterial bloom detection. *International Journal of Remote Sensing, 34*, 6668-6678

Wynne, T.T., Stumpf, R.P., Tomlinson, M.C., & Dyble, J. (2010). Characterizing a cyanobacterial bloom in western Lake Erie using satellite imagery and meteorological data. *Limnology and Oceanography, 55*, 2025-2036

Wynne, T.T., Stumpf, R.P., Tomlinson, M.C., Warner, R.A., Tester, P.A., Dyble, J., & Fahnenstiel, G.L. (2008). Relating spectral shape to cyanobacterial blooms in the Laurentian Great Lakes. *International Journal of Remote Sensing, 29*, 3665-3672

Yentsch, C.S. (1962). Measurement of visible light absorption by particulate matter in the ocean. *Limnology and Oceanography, 7*, 207-217

Zamyadi, A. (2011). The value of in vivo monitoring and chlorination for the control of toxic cyanobacteria in drinking water production. In (p. 334): University of Montreal

Zhang, F., Hu, C., Shum, C.K., Liang, S., & Lee, J. (2017). Satellite remote sensing of drinking water intakes in Lake Erie for cyanobacteria population using two MODIS-based indicators as a potential tool for toxin tracking. *Frontiers in Marine Science, 4:124. doi: 10.3389/fmars.2017.00124*

Zhao, J., Hu, C., Lenes, J.M., Weisberg, R.H., Lembke, C., English, D., Wolny, J., Zheng, L., Walsh, J.J., & Kirkpatrick, G. (2013). Three-dimensional structure of a *Karenia brevis* bloom: observations from gliders, satellites, and field measurements. *Harmful Algae, 29*, 22-30

Zieman, J., Fourqurean, J.W., & Iverson, R.L. (1989). Distribution, abundance and productivity of seagrasses and macroalgae in Florida Bay. *Bulletin of Marine Science, 44*, 292-311

1326

1327 **List of Figure Captions**

1328 Figure 1. (A) Landsat image of Florida Bay and adjacent water bodies collected on 30 December
1329 2016. Most regions in Florida Bay are less than 2m deep with many areas less than 1 m. Star
1330 symbols show locations of MODIS time-series stations. Abbreviations: N-GFB= Northern
1331 Greater Florida Bay; S-GFB = Southern Greater Florida Bay; WFB = West Florida Bay,
1332 NCFB=North Central Florida Bay, SFB = South Florida Bay, NEFB = Northeast Florida Bay,
1333 and BMB = Blackwater Sound, Manatee Bay, and Barnes Sound. NOAA station numbers are
1334 included in parenthesis. (B) Map of study area showing in situ station locations sorted by region
1335 for three independent field data sets: ＋= USF (1997-1998), ○= NOAA (2002-2012, 2016), and
1336 ×= FWC (late-2013). The solid black line represents the southern boundary for Everglades
1337 National Park.

1338

1339 Figure 2. Relationships between in situ Chl-a and (A) $a_{ph}(443)$, (B) $a_{ph}(675)$, (C) $a_d(443)$, and (D)
1340 $a_{CDOM}(443)$ for Florida Bay and adjacent water bodies in 1997-1998. Symbols represent different
1341 regions: ＋ = N-GFB, × = S-GFB, ◇ = WFB, △ = NCFB, and □ = SFB. Colors represent non-
1342 blooms (black) and blooms dominated by cyanobacteria (green) and diatoms (red). Thick solid
1343 lines represent best-fit power functions. Relationships developed previously for global oceanic
1344 (Bricaud et al., 2004) (BR04; thin solid line) and estuarine (Le et al., 2013) (LE13; dashed line)
1345 systems are shown for comparison.

1346

1347 Figure 3. In situ remote sensing reflectance spectra (sr^{-1}) for Florida Bay and adjacent water
1348 bodies in 1997-1998 sorted by region: (A) N-GFB (B) S-GFB, (C) WFB, (D) NCFB, and (E)

SFB. Colors represent non-blooms (black) and blooms dominated by cyanobacteria (green) and diatoms (red).

Figure 4. Mean in situ $R_{rs}(\lambda)$ (solid lines) and $1/a_{tot}(\lambda)$ normalized at 555nm (dashed lines) for the 1997 (A) cyanobacteria and (B) diatom blooms. Mean relative percent contribution (%) of absorbing constituents [phytoplankton (solid thick lines), detritus (dotted lines), CDOM (dashed lines), and water (solid thin lines)] to $a_{tot}(\lambda)$ for the 1997 (C) cyanobacteria and (D) diatom blooms. Shaded regions in (A,B) show the location of MODIS ocean (dark gray) and land (light gray) bands.

Figure 5. Mean in situ chlorophyll-specific phytoplankton absorption spectra, $a^*_{ph}(\lambda)$, for the 1997 cyanobacteria (solid line) and diatom (dashed line) blooms.

Figure 6. Relationship between CI_{MODIS} and SS(488) derived from in situ $R_{rs}(\lambda)$ for Florida Bay and adjacent water bodies in 1997-1998. Symbols represent different regions: + = N-GFB, × = S-GFB, ◇ = WFB, △ = NCFB, and □ = SFB. Colors represent non-blooms (black) and blooms dominated by cyanobacteria (green) and diatoms (red). The vertical dashed line represents where $CI_{MODIS} = 0$ (Wynne et al., 2013).

Figure 7. Relationships between (A) CI_{MODIS} and SS(488), (B) CI_{MODIS} and in situ Chl-a (mg m^{-3}), and (C) SS(488) and in situ Chl-a (mg m^{-3}). CI_{MODIS} and SS(488) were derived from MODIS/Aqua $R_{rc}(\lambda)$ (dimensionless) for Florida Bay and adjacent waters (NOAA; 2002-2012). Colors represent non-blooms (black), cyanobacteria blooms (green), and 'other' blooms (red).

The vertical dashed line in (A) represents where $CI_{MODIS} = 0$ (Wynne et al., 2013) and the gray shaded area represents where $CI_{MODIS} > 0$ and $SS(488) < -0.0055$.

Figure 8. In situ (A) Chl-a (mg m^{-3}) and (B) phycocyanin fluorescence (relative fluorescence units) collected on 28-29 September 2016. (C) MODIS/Terra RGB-composite image (28 September 2016) with station locations representing four distinct optical water types and mixed water types overlaid. The magenta 'X' marks a seagrass-rich, non-bloom location in S-GFB where false positive flagging of cyanobacteria blooms occurred when pixels were classified based on $CI_{MODIS} > 0$ (original CI approach; Wynne et al., 2013). (D) MODIS/Terra $R_{rc}(\lambda)$ (dimensionless) and (E) relationship between CI_{MODIS} (dimensionless) and SS(488) (dimensionless) sorted by optical water type. The vertical dashed line in (E) represents where $CI_{MODIS} = 0$ and the gray shaded area represents where $CI_{MODIS} > 0$ and $SS(488) < -0.0055$. (F-G) Classified MODIS/Terra image (28 September 2016) showing positively flagged cyanobacteria bloom pixels (green) classified according to (F) $CI_{MODIS} > 0$ (original CI approach; Wynne et al., 2013) and (G) $CI_{MODIS} > 0$ and $SS(488) < -0.0055$ (modified CI approach; this study). Non-cyanobacteria bloom pixels are shaded black, clouds are light gray, mud banks are dark gray, and land is tan.

Figure 9. MODIS/Aqua Chl_{CI} (mg m^{-3}) image series showing bloom transport in late-2013. Chl_{CI} was derived using the modified CI approach. The first date is when the image was collected. The second date (in parenthesis) indicates the in situ sampling date. Letters overlaid on the images are water sample analysis results from FWC-FWRI indicating different levels of total cyanobacteria cellular abundances (cells ml^{-1}): H= 'high' bloom ($>10^7$), M= 'medium' bloom

1395 (10^6-10^7), L= 'low' bloom (0.45 x 10^6-10^6), and N= 'non-bloom' (<0.45 x 10^6). Non-
1396 cyanobacteria bloom pixels are shaded black, clouds are light gray, mud banks are dark gray, and
1397 land is tan.
1398
1399 Figure 10. Comparison of MODIS and MERIS cyanobacteria bloom detection techniques for
1400 imagery collected on the same day. MODIS/Aqua (A) RGB, (B) Chl_{CI} (original CI approach),
1401 and (C) Chl_{CI} (modified CI approach) for 23 November 2006 (18:10 UTC). MERIS (D) RGB,
1402 (E) Chl_MPH (no cyano_flag), and (F) Chl_MPH (cyano_flag) for 23 November 2006 (15:36
1403 UTC). MERIS Chl_MPH was determined according to Matthews et al. (2012; 2015). The
1404 cyano_flag provides a means for discriminating cyanobacteria blooms from eukaryotic-
1405 dominated blooms and employs various spectral shapes (SICF, SIPF, and BAIR). The circled
1406 areas depict seagrass-rich, non-bloom waters west of the bloom that are false positively flagged
1407 as cyanobacteria blooms for MODIS Chl_{CI} when using the original CI approach (B) and MERIS
1408 Chl_MPH when the cyanobacteria flags are not applied (E).
1409
1410 Figure 11. Relationships between SS(488) derived from in situ $R_{rs}(\lambda)$ (sr^{-1}) and SS(488) derived
1411 from MODIS $R_{rc}(\lambda)$ (dimensionless) simulated based on radiative transfer theory (Eq. 3).
1412 Simulations were conducted for sensor viewing geometries at (A) scene center (θ=4°) and (B)
1413 scene edge (θ=57°) and for variable aerosol types (+: M90, ◇: C50) and aerosol optical
1414 thicknesses (black='min' (τ869=0.04) and red='max' (τ869=0.3)). The results from all
1415 simulations combined are shown in (C). The solid line represents the best-fit linear function.
1416 Uncertainty based on the mean absolute error (MAE) is also provided.
1417

1418 Figure 12. Example showing how the modified CI approach is insensitive to variable sensor
1419 viewing geometry. (a) and (b) show MODIS/Aqua RGB-composite imagery and Chl_{CI} (mg m^{-3})
1420 on 10 October 2013 (θ=21.4°). (c) and (d) show MODIS/Aqua RGB-composite imagery and
1421 Chl_{CI} (mg m^{-3}) on 11 October 2013 (θ=64.1°). The histograms in (e) show Chl_{CI} distribution
1422 statistics on 10 October 2013 (black) and 11 October 2013 (red) for areas positively classified as
1423 cyanobacteria blooms.
1424
1425 Figure 13. In situ Chl-a (mg m^{-3}) (€) and daily MODIS/Aqua Chl_{CI} (mg m^{-3}) (+) in (A) N-GFB,
1426 (B) S-GFB, (C) WFB, (D) NCFB, (E) SFB, (F) NEFB, and (G) BMB for the 2005-2008
1427 cyanobacteria bloom event. NOAA station locations (in parenthesis) are shown in Figure 1a.
1428 Chl_{CI} was set equal to zero for non-cyanobacteria bloom pixels. Black and red arrows indicate
1429 confirmed cyanobacteria and 'other' blooms, respectively. Confirmation was based on field
1430 measurements presented in this study and from previous studies (Berry et al., 2015; Garner and
1431 McCarthy, 2009; Glibert et al., 2009).
1432
1433 Figure 14. Example showing how the modified CI approach is affected by turbidity. (a) and (b)
1434 show MODIS/Aqua RGB-composite image and Chl_{CI} (mg m^{-3}) on 20 January 2017 (pre-storm
1435 with low turbidity). (c) and (d) show MODIS/Aqua RGB-composite image and Chl_{CI} (mg m^{-3})
1436 on 24 January 2017 (post-storm with high turbidity). The histograms in (e) show Chl_{CI}
1437 distribution statistics on 20 January 2017 (black) and 24 January 2017 (red) for areas positively
1438 classified as cyanobacteria blooms.